

# [Cp<sub>2</sub>TiCH<sub>2</sub>CHMe(SiMe<sub>3</sub>)]<sup>+</sup>, an Alkyl–Titanium Complex Which (a) Exists in Equilibrium between a β-Agostic and a Lower Energy γ-Agostic Isomer and (b) Undergoes Hydrogen Atom Exchange between α-, β-, and γ-Sites via a Combination of Conventional β-Hydrogen Elimination–Reinsertion and a Nonconventional CH Bond Activation Process Which Involves Proton Tunnelling

Alexandre F. Dunlop-Brière and Michael C. Baird\*

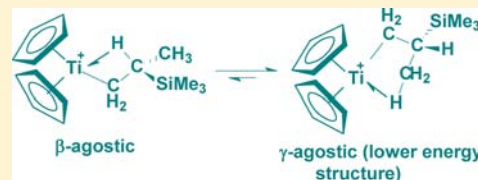
Department of Chemistry, Queen's University, Kingston, ON K7L 3N6, Canada

Peter H. M. Budzelaar\*

Department of Chemistry, University of Manitoba, Winnipeg, MB R3T 2N2, Canada

## Supporting Information

**ABSTRACT:** The compound [Cp<sub>2</sub>Ti(Me)(CD<sub>2</sub>Cl<sub>2</sub>)] [B(C<sub>6</sub>F<sub>5</sub>)<sub>4</sub>] reacts with trimethylvinylsilane (TMVS) to form the 1,2-insertion product [Cp<sub>2</sub>TiCH<sub>2</sub>CHMe(SiMe<sub>3</sub>)]<sup>+</sup> (III), which exists in solution as equilibrating β- and γ-agostic isomers. In addition, while free rotation of the β-methyl group results in a single, averaged γ-H atom resonance at higher temperatures, decoalescence occurs below ~200 K, and the resonance of the γ-agostic hydrogen atom at δ ~ -7.4 is observed. Reaction of [Cp<sub>2</sub>Ti(CD<sub>3</sub>)(CD<sub>2</sub>Cl<sub>2</sub>)]<sup>+</sup> with TMVS results in the formation of [Cp<sub>2</sub>TiCH<sub>2</sub>CH(CD<sub>3</sub>)(SiMe<sub>3</sub>)]<sup>+</sup>, which converts, via reversible β-elimination, to an equilibrium mixture of specifically [Cp<sub>2</sub>TiCH<sub>2</sub>CH(CD<sub>3</sub>)(SiMe<sub>3</sub>)]<sup>+</sup> and [Cp<sub>2</sub>TiCD<sub>2</sub>CD(CH<sub>3</sub>)(SiMe<sub>3</sub>)]<sup>+</sup>. Complementing this conventional process, exchange spectroscopy experiments show that the β-H atom of [Cp<sub>2</sub>TiCH<sub>2</sub>CHMe(SiMe<sub>3</sub>)]<sup>+</sup> undergoes exchange with the three hydrogen atoms of the β-methyl group (β-H/γ-H exchange) but *not* with the two α-H atoms. This exchange process is completely shut down when [Cp<sub>2</sub>TiCH<sub>2</sub>CH(CD<sub>3</sub>)(SiMe<sub>3</sub>)]<sup>+</sup> is used, suggesting an H/D kinetic isotope effect much larger (apparently >16 000) than the maximum possible for an over-the-barrier process. It is proposed that β-H/γ-H exchange is facilitated by quantum mechanical proton tunnelling in which a hydrogen atom of the 2-methyl group of the alkene–hydride deinsertion product [Cp<sub>2</sub>TiH{CH<sub>2</sub>=CMe(SiMe<sub>3</sub>)}]<sup>+</sup> undergoes reversible exchange with the hydride ligand via the allyl dihydrogen species [Cp<sub>2</sub>TiH<sub>2</sub>{(η<sup>3</sup>-CH<sub>2</sub>C(SiMe<sub>3</sub>)CH<sub>2</sub>)}]<sup>+</sup>. Complementing these findings, DFT calculations were carried out to obtain energies and NMR parameters for all relevant species and thence to obtain better insight into the agostic preference(s) of complex III and the observed exchange processes. In all cases where comparisons between experimental and calculated data were possible, agreement was excellent.



## INTRODUCTION

There has in recent years been considerable interest in the utilization of metallocene complexes of the types Cp<sub>2</sub>M(Me)-(WCA) or [Cp<sub>2</sub>M(Me)(solvent)]WCA [M = Ti(IV), Zr(IV), Hf(IV); Me = methyl; WCA = weakly coordinating anion such as B(C<sub>6</sub>F<sub>5</sub>)<sub>4</sub><sup>-</sup>] as catalysts for the coordination polymerization of alkenes CH<sub>2</sub>=CHR (R = H, alkyl, aryl).<sup>1</sup> It is universally accepted that the initial steps of such polymerization processes involve coordination of the alkene to generate a cationic intermediate [Cp<sub>2</sub>M(Me)(η<sup>2</sup>-CH<sub>2</sub>=CHR)]<sup>+</sup> (A), which undergoes subsequent migratory insertion to give an alkyl intermediate of type B (vacant site possibly occupied by alkene, solvent molecule, or WCA).

Until recently, NMR studies of d<sup>0</sup> metallocene-based alkene polymerization catalyst systems had never provided direct

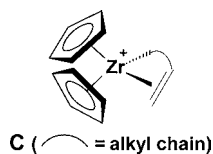


evidence for alkyl alkene intermediates such as type A, presumably because (a) a lack of π back-donation from d<sup>0</sup> metal ions results in weak alkene-metal bonding and (b) activation energies for migratory insertion processes involving, for example, ethylene, propylene, and 1-alkenes are very low. Thus species of type A are too short-lived to be observed,

Received: September 7, 2013

Published: October 22, 2013

although complexes of type C, stabilized by chelation and other means, have been reported.<sup>2</sup>



In C, tethering of the alkene apparently prevents rearrangement to the four-centered transition state necessary for migratory insertion to occur.

As we have recently observed, however, there is an alternative to tethering, as in C, to make possible the observation of alkyl alkene complexes of type A: one can utilize alkenes that do not readily undergo migratory insertion reactions, i.e., are generally nonpolymerizable via a coordination polymerization process.<sup>3</sup> Thus, for instance,  $[\text{Cp}_2\text{Zr}(\text{Me})(\text{CD}_2\text{Cl}_2)][\text{B}(\text{C}_6\text{F}_5)_4]$  reacts with 2,4-dimethyl-1-pentene (DMP) to form  $[\text{Cp}_2\text{Zr}(\text{Me})(\text{DMP})][\text{B}(\text{C}_6\text{F}_5)_4]$ , which can be studied via NMR spectroscopy at low temperatures.<sup>3</sup> DFT calculations suggested that the activation energy for migratory insertion of the DMP ligand is relatively high, largely because the two substituents on C(2) provide steric hindrance which raises the energy of the migratory insertion transition state.<sup>3</sup> Thus,  $[\text{Cp}_2\text{Zr}(\text{Me})(\text{DMP})]^+$  was characterized by a series of low-temperature 1D and 2D NMR experiments, supported by DFT calculations, which suggested that the alkene bonding mode is highly asymmetric, with the Zr–C(1) distance being significantly shorter than the Zr–C(2) distance and, apparently, a high degree of carbocationic nature for C(2). Thus, the structure appears to be described more appropriately as in **b** of Figure 1, analogous to intermediates during carbocationic polymerization of 2,2-disubstituted 1-alkenes,<sup>4</sup> rather than as the conventional  $\eta^2$  structure **a**.

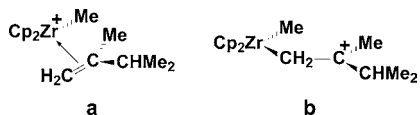
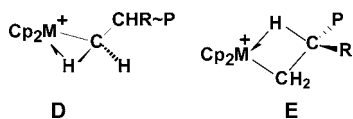


Figure 1. Alternative structures of  $[\text{Cp}_2\text{Zr}(\text{Me})(\text{DMP})]^+$ .

Consistent with this hypothesis, there occurs rotation of the  $\text{R}(\text{Me})\text{C}=\text{C}$  group along the C(1)–C(2) axis and relative to the  $=\text{CH}_2$  group, implying significant loss of C=C double bond character in the near- $\eta^1$  coordinated alkene.<sup>3</sup>

During a coordination polymerization process, propagation following the formation of **B** involves a succession of analogous alkene coordination and migratory insertion steps, the insertions being facilitated by  $\alpha$ -agostic interactions as in **D** ( $\text{P}$  = polymeryl) with complementary  $\beta$ -agostic species (**E**) serving as resting states during propagation.<sup>5</sup>

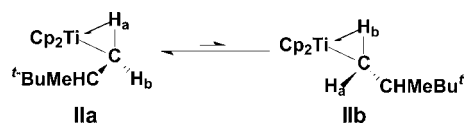


The  $\alpha$ - and  $\beta$ -agostic modes of bonding, denoted by the half arrows in **D** and **E**, involve donation of electron density from respectively delocalized H–C(1) and H–C(2)–C(1)  $\sigma$  bonding molecular orbitals to a vacant orbital on the highly Lewis acidic metal ion.<sup>5</sup> Agostic complexes are well-known for late transition metal compounds,<sup>5qr</sup> and a small number of  $\beta$ -agostic

zirconocene complexes of the type  $[\text{Cp}_2\text{ZrRL}]^+$  ( $\text{R} = \text{Et}, \text{CH}_2\text{CH}_2\text{Ph}, \text{CH}_2\text{CH}_2\text{CMe}_3, \text{CH}_2\text{CHMe}_2$ ;  $\text{L} = \text{PMe}_3, \text{MeCN}$ ) are known.<sup>6a,b,d</sup> Zirconocene(IV) complexes containing  $\alpha$ -agostic interactions of type **D** seem to be unknown and titanocene(IV) complexes containing  $\alpha$ - or  $\beta$ -agostic complexes of types **D** and **E** have also until very recently<sup>6e,f</sup> not been characterized. As with species of types **A** and **B**, activation energies for migratory insertion processes involving readily polymerized alkenes such as ethylene, propylene, and 1-alkenes are sufficiently low that lifetimes of species **D** and **E** are too short for them to be observed.

Recognizing, as outlined above, that coordination of alkenes which are nonpolymerizable via a coordination polymerization process can generate  $d^0$  metal–alkene complexes which are sufficiently stable at low temperatures that they can be characterized and studied, we attempted to synthesize the analogous titanocene(IV) complex  $[\text{Cp}_2\text{Ti}(\text{Me})(\text{DMP})]^+$  by reacting DMP with  $[\text{Cp}_2\text{Ti}(\text{Me})(\text{CD}_2\text{Cl}_2)][\text{B}(\text{C}_6\text{F}_5)_4]$  (**I**). Instead, we obtained, via a complex cascade of reactions, the cationic species  $[\text{Cp}_2\text{Ti}(\text{CH}_2\text{CHMeCH}_2\text{CHMe}_2)]^+$ , identified as a  $\beta$ -agostic metal–alkyl complex of type **E**.<sup>6e</sup> The new complex was characterized by the complete analysis of a series of 1D and 2D NMR spectra, and a mechanism for its formation which involved an  $\varepsilon$ -agostic intermediate and a 1,5 metal shift was formulated on the basis of DFT calculations.<sup>6e</sup>

Pursuing this theme, we subsequently investigated the reaction of **I** with another type of sterically hindered alkene, 3,3-dimethyl-1-butene (3,3-DMB). This alkene also seems not to be known to undergo homopolymerization via a coordination polymerization mechanism,<sup>6f</sup> and it therefore seemed likely that multiple insertion reactions would again be difficult and that it might be possible once more to study interesting alkene and/or agostic complexes. Reaction proceeded readily in  $\text{CD}_2\text{Cl}_2$  at 195–205 K but resulted, via an  $\eta^2$ -3,3-DMB complex according to DFT calculations, in the formation of a *single insertion*,  $\alpha$ -agostic metal–alkyl complex,  $[\text{Cp}_2\text{TiCH}_2\text{CHMe}^t\text{Bu}]^+$  (**II**), of type **D**. Interestingly, although the diastereotopic  $\alpha$ -CH<sub>2</sub> protons could not undergo mutual exchange, NMR spectral evidence and DFT calculations suggested that they alternated between agostic and nonagostic positions, i.e., that **II** equilibrated between structures **IIa** and **IIb** in a windshield-wiper-like fashion.<sup>6f</sup>



The fact that  $\alpha$ -H(a) and  $\alpha$ -H(b) exhibited very different chemical shifts and  $^1J_{\text{CH}}$  coupling constants suggested, however, that one of these conformations was strongly preferred. Characteristic of the agostic hydrogen atoms in these titanocene compounds are their negative  $^1\text{H}$  NMR chemical shifts, resulting from ring current effects from the Cp rings; nonmetallocene group 4 agostic compounds exhibit positive  $^1\text{H}$  NMR chemical shifts.<sup>6e,f</sup>

The  $\alpha$ -agostic structure observed for **II** was also very interesting because most coordinatively unsaturated metal–alkyl compounds bearing  $\beta$ -H atoms prefer  $\beta$ - over  $\alpha$ -agostic structures.<sup>5,6a–c,7</sup> However, DFT calculations suggested that the  $\beta$ -agostic structure of **II** is destabilized by steric factors arising from the presence of the methyl and *t*-Bu groups on the  $\beta$ -carbon atom; a  $\beta$ -agostic structure would force the methyl and *t*-Bu groups into close proximity to the Cp rings, generating

repulsive contacts which are avoided in the  $\alpha$ -agostic structures. The promotion of  $\alpha$ - over  $\beta$ -agostic structures by steric factors had been observed with other ligand systems,<sup>5,7</sup> but our results clearly demonstrated the delicate balance between electronic factors ( $\beta$ -agostic generally preferred) and steric effects ( $\beta$ , $\beta$ -disubstitution favoring  $\alpha$ -agostic conformations as in **II**) for highly unsaturated and reactive alkyl metallocenium cations. Furthermore, as noted above, utilization of alkenes which do not readily undergo coordination polymerization makes possible studies of normally unobservable  $\alpha$ - and  $\beta$ -agostic intermediate species. In these cases, barriers to subsequent monomer insertion steps are sufficiently high that important intermediates can be observed and characterized at low temperatures.

We now report a similar study of the reaction of **I** with trimethylvinylsilane (TMVS), another alkene which seems not to be readily polymerized via coordination polymerization processes,<sup>8</sup> although a few rather "normal"  $\eta^2$ -complexes are known;<sup>9a-d</sup> in addition, copolymerization with ethylene, presumably via a coordination polymerization process, has been reported.<sup>9e</sup> Given the similarity of TMVS to 3,3-DMB, we anticipated further opportunities to study agostic species, and we have not been disappointed.

## EXPERIMENTAL SECTION

All syntheses were carried out under dry, deoxygenated argon using standard Schlenk line techniques, using argon deoxygenated by passage through a heated column of BASF copper catalyst and then dried by passing through a column of activated 4A molecular sieves, or an MBraun Labmaster glovebox. NMR spectra were recorded using a Bruker AV600 spectrometer, <sup>1</sup>H, <sup>2</sup>H, and <sup>13</sup>C NMR data being referenced to TMS via the residual proton signals of the solvent. [Ph<sub>3</sub>C][B(C<sub>6</sub>F<sub>5</sub>)<sub>4</sub>] was purchased from Asahi Glass Co. and used as obtained, while CH<sub>3</sub>Li, CD<sub>3</sub>Li, and trimethylvinylsilane (TMVS) were purchased from Aldrich. Cp<sub>2</sub>TiMe<sub>2</sub> was synthesized from Cp<sub>2</sub>TiCl<sub>2</sub> and CH<sub>3</sub>Li, as described previously,<sup>6e,f</sup> and was stored in ethyl ether solution (~40.5 mM) under argon at -30 °C. Dichloromethane-*d*<sub>2</sub> was dried by storage over activated 3A molecular sieves.

Solutions containing [Cp<sub>2</sub>Ti(Me)(CD<sub>2</sub>Cl<sub>2</sub>)] [B(C<sub>6</sub>F<sub>5</sub>)<sub>4</sub>] (**I**) for NMR studies were prepared as follows. An aliquot of Cp<sub>2</sub>TiMe<sub>2</sub> in ethyl ether (0.7 mL, ~0.03 mmol) was taken from the stock solution, the solvent was removed quickly, and the residue was dissolved in 0.5 mL of CD<sub>2</sub>Cl<sub>2</sub>. To this was added a solution of [Ph<sub>3</sub>C][B(C<sub>6</sub>F<sub>5</sub>)<sub>4</sub>] (35–55 mg, ~0.04–0.06 mmol) in 0.6 mL of CD<sub>2</sub>Cl<sub>2</sub> in the glovebox. The mixture was then syringed into a rubber septum sealed NMR tube, and the NMR tube was taken quickly out of the glovebox and immersed within 2 min in a dry ice/acetone bath (195 K). The NMR tube was placed in the precooled (185–205 K) probe of the NMR spectrometer, and a <sup>1</sup>H NMR spectrum was run. The tube was then removed from the probe to the dry ice/acetone bath, and aliquots of the TMVS (molar ratio I:alkene ≈ 1:0.5 to 1:1.1) were added to the cold solution. The tube was shaken vigorously at 195 K to induce mixing and placed back in the probe at 185–215 K, and NMR spectra were obtained at various time intervals and temperatures. Note that although solutions of **I** prepared as above always contained relatively small amounts of [Cp<sub>2</sub>TiMe{B(C<sub>6</sub>F<sub>5</sub>)<sub>4</sub>}]<sup>6e,f</sup> the latter did not react with TMVS under the experimental conditions used here.

Geometry optimizations were carried out with Turbomole<sup>10a,b</sup> using the TZVP basis<sup>10c</sup> and the b-p functional<sup>10d-f</sup> (without RI approximation) in combination with an external optimizer (PQS OPTIMIZE).<sup>10j,k</sup> Vibrational analyses were carried out for all stationary points to confirm their nature (one imaginary frequency for transition states, none for minima). Final energies were obtained using the TZVPP basis<sup>11a</sup> and a COSMO solvent correction ( $\epsilon = 9.1$ , CH<sub>2</sub>Cl<sub>2</sub>).<sup>11b</sup> These were combined with thermal corrections (enthalpy and entropy, 225 K, 1 bar) from the TZVP vibrational analyses to arrive at the final free energies. To account for the reduced freedom of

movement in solution, entropy contributions to the free energies were scaled to two-thirds of their gas-phase values.<sup>11c,d</sup> To evaluate the sensitivity to method and basis sets, separate calculations were carried out (1) following the same procedure but with the b3-lyp<sup>10f-i</sup> functional used throughout and (2) by recalculation at the b-p/TZVP geometries of improved single-point energies using Gaussian,<sup>11e</sup> the M06 functional, the (m)aug-cc-pVTZ basis set,<sup>12,13</sup> and a PCM (dichloromethane) solvent correction. The results of these test calculations did not differ dramatically from the b-p/TZVPP/COSMO//b-p/TZVP results, and therefore, only the latter will be discussed in the text.

We found earlier that prediction of NMR parameters works better when using a hybrid functional, and therefore separate optimizations were carried out at the b3-lyp/TZVP level, followed by evaluation of chemical shifts (GIAO method<sup>10m-p</sup>) and scalar coupling constants<sup>10q-t</sup> using Gaussian, a TZVP basis set on Ti, and the IGLO-III<sup>11f</sup> basis set on Si, C, and H, in combination with the functional B3LYP.<sup>10g,i,l</sup> The counteranion used experimentally, [B(C<sub>6</sub>F<sub>5</sub>)<sub>4</sub>]<sup>-</sup>, was not included in the calculations because it is not currently feasible to explore the many relative orientations of cation and anion which are possible and then average the results to obtain chemical shifts. In any case, in a relatively polar solvent like dichloromethane, ion pair association would be expected to be relatively loose and the agreement between observed and calculated chemical shifts is such that the counteranion does not appear to greatly influence the NMR parameters of the cation. For full results of the calculations, see Tables S1–S4 in the Supporting Information.

## RESULTS AND DISCUSSION

**NMR Evidence for Agostic Structures.** The species obtained in reactions of Cp<sub>2</sub>TiMe<sub>2</sub> with a slight excess of [Ph<sub>3</sub>C][B(C<sub>6</sub>F<sub>5</sub>)<sub>4</sub>] have been described previously.<sup>6e,f</sup> In addition to Ph<sub>3</sub>CMe, the product of methyl carbanion abstraction, mixtures of the solvent separated, ionic [Cp<sub>2</sub>Ti(Me)(CD<sub>2</sub>Cl<sub>2</sub>)] [B(C<sub>6</sub>F<sub>5</sub>)<sub>4</sub>] (**I**), and the contact ion pair [Cp<sub>2</sub>TiMe{B(C<sub>6</sub>F<sub>5</sub>)<sub>4</sub>}] are formed, and it is the former which reacts with alkenes. Bright yellow NMR samples were prepared as described in the Experimental Section and were placed in the probe of a 600 MHz NMR spectrometer preset to 205 K. The <sup>1</sup>H NMR spectra were found to exhibit resonances of the products: CMePh<sub>3</sub> at  $\delta$  7.0–7.3 (m), 2.13 (s); **I** at  $\delta$  6.72 (Cp), 1.63 (Me); [Cp<sub>2</sub>TiMe{B(C<sub>6</sub>F<sub>5</sub>)<sub>4</sub>}] at  $\delta$  6.33 (Cp), 1.24 (Me) (see the Supporting Information, Figure S1b).

The addition of a substoichiometric amount of TMVS to a mixture of **I** and [Cp<sub>2</sub>TiMe{B(C<sub>6</sub>F<sub>5</sub>)<sub>4</sub>}] in CD<sub>2</sub>Cl<sub>2</sub> at 195 K followed by raising the temperature to 215 K resulted in weakening of the resonances of **I** and the appearance of well-resolved resonances at  $\delta$  6.07 (s, 10H), 4.41 (m, 1H), 4.30 (m, 1H), 0.21 (s, 9H), and -0.36 (m, 1H) (Supporting Information, Figures S1c and S2), attributable to a new species, **III**. The resonances at  $\delta$  6.07 and 0.21 are clearly to be attributed to Cp and Me<sub>3</sub>Si groups, respectively, and the others to single hydrogen atoms on C(1) ( $\alpha$ -H<sub>a</sub>,  $\alpha$ -H<sub>b</sub>) and C(2) ( $\beta$ -H); the negative chemical shift suggests that one of them might be agostic.<sup>6e,f</sup> We were surprised not to observe a 3H resonance for the  $\beta$ -methyl group ( $\gamma$ -H), but on raising the temperature above 205 K, a very broad, 3H resonance began to appear at  $\delta$  ~ -0.7 to -0.9; this shifted to lower field and narrowed as the temperature was raised to 250 K. Concurrently with these changes, the resonance at  $\delta$  -0.36 shifted upfield, and at 270 K, the two resonances had crossed over and the 3H methyl resonance had decoalesced to a doublet ( $J = 6.9$  Hz) (Figure 2).

Full consideration of the structural and dynamic exchange implications of a series of 1D and 2D NMR experiments at

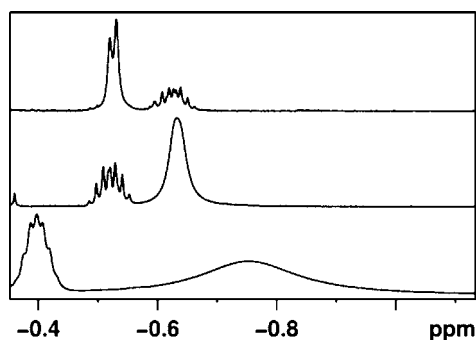


**Figure 2.** Changes in the  $^1\text{H}$  NMR spectrum of **III** in the temperature range 225 K (bottom), 250 K (middle), and 270 K (top).

various temperatures, complemented by DFT calculations, is presented below. One readily concludes that **III** is to be identified as  $[\text{Cp}_2\text{TiCH}_2\text{CHMe}(\text{SiMe}_3)]^+$ , the product of a single 1,2-insertion of TMVS into the Ti–Me bond of **I** (Scheme 1).

Because **C(2)** is chiral, the pair of hydrogen atoms on **C(1)**,  $\alpha\text{-H}_a$  and  $\alpha\text{-H}_b$ , are diastereotopic, explaining the observation of separate resonances for these hydrogen atoms and hence the presence of three  $^1\text{H}$  resonances. COSY spectra over a range of temperatures exhibit correlations between the resonances at  $\delta$  4.41, 4.30, and  $-0.36$  (Supporting Information, Figure S3), and the mutual couplings of 8.7 Hz between the resonances at  $\delta$  4.41 and 4.30 confirm assignments of these to  $\alpha\text{-H}_a$  and  $\alpha\text{-H}_b$ . Although the very broad  $\beta$ -methyl resonance exhibits no COSY correlations below about 245 K, it does exhibit a correlation ( $^3J = 6.9$  Hz) at higher temperatures with the resonance at  $\delta -0.36$  (Supporting Information, Figure S4), which is attributed to the  $\beta\text{-H}$  atom on **C(2)**. The latter resonance also exhibits quite different vicinal couplings to the  $\alpha\text{-CH}$  resonances at  $\delta$  4.41 (7.9 Hz) and 4.30 (12.7 Hz), suggesting that the two vicinal angles of the dominant agostic structure are quite different. Experimental chemical shift and coupling constant data for **III** at 215 K are given in Table 1, where they are compared with data calculated for the  $\gamma$ -agostic isomer of **III** (see below and Supporting Information, Table S3).

The temperature dependences evident in Figure 2 are reflected in the NMR parameters in general. Thus, the Cp and  $\text{Me}_3\text{Si}$  resonances shift downfield to  $\delta$  6.14 and 0.26, respectively, on raising the temperature to 250 K. The  $\alpha\text{-CH}$  resonances also shift downfield, albeit at different rates, and overlap significantly at  $\delta \sim 4.4$  at 250 K, although there is no change in the  $\alpha\text{-CH}_a\text{-}\alpha\text{-CH}_b$  geminal coupling constant. The vicinal coupling of 12.6 Hz between  $\alpha\text{-H}_b$  and  $\beta\text{-H}$  remains essentially unchanged in the temperature range 215–250 K, but that between  $\alpha\text{-H}_a$  and  $\beta\text{-H}$  decreases from 7.8 to 7.4 Hz and that between  $\beta\text{-H}$  and the  $\beta\text{-Me}$  hydrogens decreases from 6.9 to 6.8 Hz over the same temperature range. In addition,  $^1J_{\text{CH}}$  for the  $\beta\text{-H}$  atom of **III** is 131, 133, and 137 Hz at 205, 225, and 250 K, respectively, but that of  $[\text{Cp}_2\text{TiCH}_2\text{CH}(\text{CD}_3)(\text{SiMe}_3)]^+$  (**III-d<sub>3</sub>**; see below) is 128 Hz at 225 K and 130 Hz at 250 K,

while  $^1J_{\text{CH}}$  of the methyl resonances of **III** and **III-d<sub>3</sub>** (see below) at 250 K are  $\sim 133$  and 126 Hz, respectively. These differences are all quite small, but several appear to be significant and suggest that the NMR parameters are to be interpreted as weighted averages of two or more species involved in temperature-dependent equilibria.

Observation of negative chemical shifts for the resonances of the  $\beta\text{-H}$  atom and the  $\beta$ -methyl group suggests that these hydrogen atoms experience  $\beta$ - and  $\gamma$ -agostic character, respectively, and the observed variations of chemical shifts as the temperature changes (Figure 2) suggest that there is equilibration between  $\beta$ - and  $\gamma$ -agostic structures, with the latter being unexpectedly<sup>5,6a-c,7</sup> of lower energy as indicated in Scheme 2.

Interestingly, the extreme broadening of the resonance of the three  $\gamma\text{-H}$  atoms of the  $\beta$ -methyl group suggests that they are exchanging between nonequivalent positions at intermediate temperatures; presumably, one of the methyl hydrogen atoms is  $\gamma$ -agostic at any one time. Consistent with this conclusion, reduction of the temperature below 205 K resulted in decoalescence of the broad methyl resonance shown in Figure 2 and, below 180 K, a broad new  $^1\text{H}$  resonance appeared at  $\delta \sim -7.4$  (Figure 3).

This resonance exhibited correlations in a NOESY experiment with a partially obscured  $^1\text{H}$  resonance at  $\delta \sim 3.0$  and a similar but completely obscured resonance at  $\delta \sim 1.5$ . These results are consistent with the presence of two diastereotopic, nonagostic methyl hydrogen atoms, with normal chemical shifts, and a  $\gamma$ -agostic hydrogen atom (chemical shift of  $\delta \sim -7.4$ ), with a sufficiently strong agostic bond to titanium that methyl rotation is slow on the NMR time scale at this low temperature. Supporting this conclusion, DFT calculations suggest that the chemical shifts of the agostic and the two nonagostic hydrogen atoms are  $\delta -7.2$ , 2.9, and 1.4, respectively (average  $\delta -0.9$ ; compare with Figure 2).

With the calculated chemical shifts of the agostic and nonagostic  $\gamma\text{-H}$  atoms in  $\gamma$ -agostic **III** in hand (see above and footnote *c* of Table 1), we calculated also (see Supporting Information, Table S3) the chemical shifts of the nonagostic  $\beta\text{-H}$  atom in  $\gamma$ -agostic **III** ( $\delta$  0.03) and of the agostic  $\beta\text{-H}$  atom ( $\delta -4.34$ ) and nonagostic  $\gamma\text{-H}$  atoms (average  $\delta$  1.76) of  $\beta$ -agostic **III**. Assuming that the intrinsic chemical shifts are temperature-independent and that the observed chemical shifts are weighted averages of the two exchanging species in Scheme 2, we have utilized the experimental and computed chemical shift data to determine the equilibrium constants for isomerization between the  $\beta$ -agostic **III** and  $\gamma$ -agostic **III** isomers at several temperatures and thence to determine thermodynamic data for the isomerization reaction. From a linear regression of  $\Delta G = \Delta H - T\Delta S$  (deduced from equilibrium constants) vs temperature, we find  $\Delta G$  for the conversion of  $\beta$ -agostic **III** to  $\gamma$ -agostic **III** to be  $-0.59$  kcal/mol at 225 K compared with a calculated value of  $-1.9$  kcal/mol (see below). In addition,  $\Delta H$  for the  $\beta$ -agostic to  $\gamma$ -agostic conversion is  $-1.79 \pm 0.05$  kcal/mol, and  $\Delta S$  is  $-5.3 \pm 0.5$  cal/mol·K, with  $R^2 = 0.9924$ .

#### Scheme 1. Formation of **III** via the Reaction of **I** with TMVS

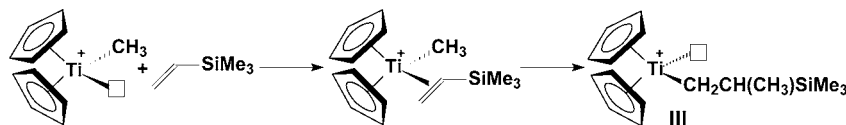


Table 1. Observed and Calculated (for  $\gamma$ -agostic structure) NMR Data for III at 215 K

group	$^1\text{H}$		$^{13}\text{C}$ ( $^1J_{\text{CH}}$ ) <sup>a</sup>		other	
	expl	calcd	expl	calcd	expl	calcd
$\alpha\text{-H}_a$	4.41	4.78	102.9 (150)	107.5 (148.3)	$^2J_{\text{HH}} = 8.9, ^3J_{\text{HH}} = 7.8$	$^2J_{\text{HH}} = -9.5, ^3J_{\text{HH}} = 7.3$
$\alpha\text{-H}_b$	4.31	4.77	102.9 (147)	107.5 (142.7)	$^2J_{\text{HH}} = 8.9, ^3J_{\text{HH}} = 12.6$	$^2J_{\text{HH}} = -9.5, ^3J_{\text{HH}} = 13.1$
$\beta\text{-H}$	-0.36	0.03	-1.8 (133)	7.7 (124.8)	$^3J_{\text{HH}} = 12.6, 7.8, 6.9$	$^3J_{\text{HH}} = 13.1, 7.3, 7.0$
$\beta\text{-Me}$	-0.78	-0.94 <sup>c</sup>	34 (133) <sup>d</sup>	34.2 (122.6)	$^3J_{\text{HH}} = 6.9$	$^3J_{\text{HH}} = 7.0$
$\text{Me}_3\text{Si}^b$	0.21	0.42	-2.2 (122)	-0.8		
Cp	6.07	6.23	112.3	124.4		

<sup>a</sup> $^{13}\text{C}$  data from HSQC and HMBC spectra shown in Supporting Information, Figures S5–S7. <sup>b</sup> $^{29}\text{Si}$  resonance was observed at  $\delta -22.3$  ( $^1\text{H}$ – $^{29}\text{Si}$  HMBC; see Supporting Information, Figure S8). <sup>c</sup>Calculated individual shifts:  $\delta$  2.9, 1.4, -7.2 (see Figure 3). <sup>d</sup> $^1J$  determined at 250 K.

### Scheme 2. Exchange between $\beta$ - and $\gamma$ -Agostic Isomers of III via the Nonagostic Isomer

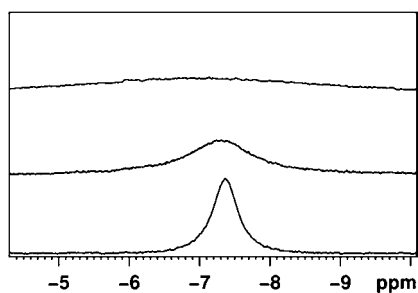
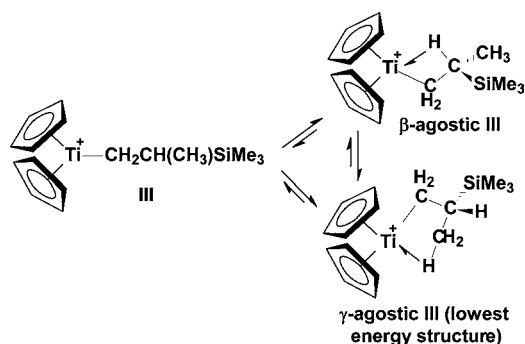


Figure 3.  $^1\text{H}$  NMR spectra of  $[\text{Cp}_2\text{TiCD}_2\text{CDCH}_3(\text{SiMe}_3)]^+$  ( $\delta$  -4.5 to -10) at 190 K (top), 181 K (middle), and 172 K (bottom), showing emergence of the resonance of the agostic hydrogen as the temperature decreases.

Although agostic  $\beta$ -methyl groups in ethyltitanium complexes have been characterized crystallographically, such compounds are fluxional in solution and only fully coalesced, dynamic NMR spectra have previously been observed.<sup>5m</sup> In contrast, cobalt(III) and palladium(II) complexes of the types  $[\text{CpCoL}(\text{CH}_2\text{CH}_3)]^+$  and  $[\text{Pd}(\alpha\text{-diimine})(\text{CH}_2\text{CH}_3)]^+$  contain  $\beta$ -methyl groups for which NMR evidence of restricted methyl rotation has been obtained.<sup>5q,r</sup> Cooling solutions of these to  $\sim 200$  or  $\sim 143$  K, respectively, results in decoalescence of the  $\beta$ -methyl resonances to three distinct, single hydrogen atom resonances, one of which exhibits a high field chemical shift and a much reduced value of  $^1J_{\text{CH}}$ , both characteristic of a  $\beta$ -agostic hydrogen atom and similar to the behavior of III, although the latter could not be studied at temperatures sufficiently low that  $^1J_{\text{CH}}$  could be determined.

**Additional, Unanticipated Exchange Processes.** Consistent with the assignments in Table 1, NOESY experiments run at various temperatures (Supporting Information, Figures S9–S15) generally exhibited positive NOE correlations

between the resonances of  $\alpha\text{-H}_a$ ,  $\alpha\text{-H}_b$ , and  $\beta\text{-H}$  and the Cp and  $\text{SiMe}_3$  groups. Surprisingly, however, the  $\beta$ -methyl resonance exhibited a *negative* correlation with the resonance of the  $\beta\text{-H}$  atom, as is clear from Figure 4 (inset of Figure S10

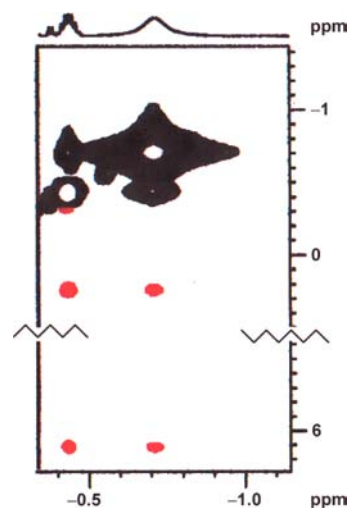
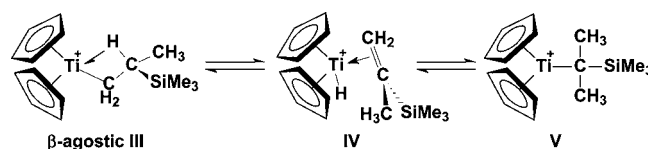


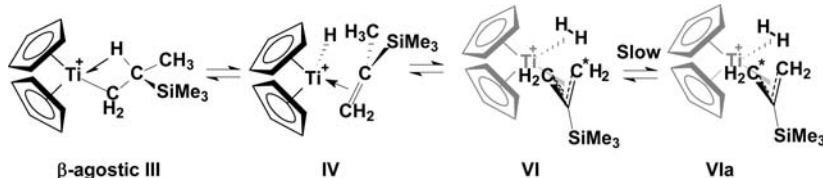
Figure 4. Partial NOESY spectrum of III at 235 K, showing the negative exchange spectroscopy (EXSY) correlations between the broad resonances of the  $\beta\text{-H}$  and the  $\gamma\text{-H}$  atoms at  $\delta -0.43$  and  $-0.71$ , respectively; NOEs with the relatively narrow  $\text{SiMe}_3$  and Cp resonances at  $\delta 0.25$  and  $6.1$ , respectively, are also apparent. For the full spectrum, see the Supporting Information (Figure S10).

of the Supporting Information). This result implies an exchange process (quite different from that shown in Scheme 2) in which the  $\beta\text{-H}$  atom undergoes exchange with the three hydrogen atoms of the  $\beta$ -methyl group ( $\beta\text{-H}/\gamma\text{-H}$  exchange) but *not* with the two  $\alpha\text{-H}$  atoms. At first sight the apparent hydrogen atom exchange might seem to be rationalized on the basis of reversible  $\beta\text{-H}$  elimination to give first an alkene hydride species IV and thence a symmetric tertiary alkyl isomer V (Scheme 3).

However, since the two  $\alpha$ -methyl groups of the intermediate V are identical, any of the six  $\beta\text{-H}$  atoms could migrate to

### Scheme 3. $\beta$ -Elimination Mechanism for Exchange between the $\beta\text{-H}$ Atom and the Hydrogen Atoms of the $\beta$ -Methyl Group

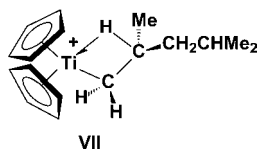


Scheme 4. Allylic Dihydrogen Mechanism for Exchange between the  $\beta$ -H Atom and the Hydrogen Atoms of the  $\beta$ -Methyl Group

titanium to regenerate **IV**, and since two of the hydrogen atoms of one of the methyl groups of **V** are derived from the  $\alpha$ -CH<sub>2</sub> group, this process would result in exchange of the  $\beta$ -H and  $\beta$ -Me atoms with the  $\alpha$ -H atoms also. Since no EXSY correlation involving the  $\alpha$ -CH<sub>2</sub> group is observed in the temperature range 215–245 K, the mechanism shown in Scheme 3 cannot apply.

An alternative process would involve isomerization of **III** via CH activation of the  $-\text{CH}_2\text{CHMeSiMe}_3$  ligand to give the allylic dihydrogen species **VI** as in Scheme 4. Similar transformations have been hypothesized to occur during metallocene-catalyzed propylene polymerization in order to account for the formation of dormant allylic species and the concomitant formation of H<sub>2</sub> as a byproduct,<sup>1b,5j,14</sup> and we note that rotation of the methyl group of **IV** and of the dihydrogen ligand of **VI** would enable exchange of both of the hydrogen atoms of the latter with the hydrogen atoms of the methylene group proximal to the H<sub>2</sub> ligand (C\*H<sub>2</sub>). In contrast, exchange involving the  $\alpha$ -CH<sub>2</sub> group of **III** would require reorganization of **VI** to **VIa**, and this may well be a relatively slow process given that the three receptor orbitals of the bent Cp<sub>2</sub>Ti(IV) fragment (1a<sub>1</sub>, b<sub>2</sub>, 2a<sub>1</sub>) all lie in the plane perpendicular to the Cp–Ti–Cp plane.<sup>15</sup> Thus, the termini of the allyl ligand should remain nonequivalent, as shown, and this would result in exchange involving the hydrogen atoms of the  $\alpha$ -CH<sub>2</sub> group being slower, as is observed.

Although the similar complex [Cp<sub>2</sub>TiCH<sub>2</sub>CHMe<sup>t</sup>Bu]<sup>+</sup> (**II**), which assumes an  $\alpha$ -agostic lowest energy structure,<sup>6f</sup> does not appear to exhibit analogous  $\beta$ -H/ $\gamma$ -H exchange at 215 K, we have previously observed exchange at 205 K between the  $\beta$ -H atom, the three  $\gamma$ -H atoms of the  $\beta$ -methyl group, two hydrogen atoms of the  $\alpha$ -CH<sub>2</sub> group, and the six hydrogen atoms of the two terminal methyl groups of the compound [Cp<sub>2</sub>Ti(CH<sub>2</sub>CHMeCH<sub>2</sub>CHMe<sub>2</sub>)]<sup>+</sup> (**VII**).<sup>6e</sup>



Consistent with the mechanism shown in Scheme 4, **VII** also underwent degradation to the corresponding allylic compound [Cp<sub>2</sub>Ti{ $\eta$ <sup>3</sup>-(CH<sub>2</sub>)<sub>2</sub>CCH<sub>2</sub>CHMe<sub>2</sub>}]<sup>+</sup> and, presumably, H<sub>2</sub> although the latter was not detected. Reversible  $\beta$ -H elimination–reinsertion and allylic dihydrogen mechanisms, analogous to those shown in Schemes 3 and 4, respectively, were considered for this system also and circumstantial evidence that the latter pertains was obtained although a computational study found in favor of the  $\beta$ -H elimination–reinsertion mechanism of Scheme 3.

While exchange of the  $\beta$ -Me and the  $\beta$ -H atoms with the hydrogen atoms of the  $\alpha$ -CH<sub>2</sub> group is not apparent in NOESY spectra in the temperature range 215–245 K, close inspection of NOESY spectra run at 255 and 260 K (Supporting

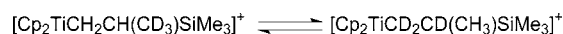
Information, Figures S12 and S14) does reveal negative EXSY correlations between the resonance of the  $\beta$ -methyl group and the resonances of the  $\alpha$ -CH<sub>2</sub> group, which have converged at this temperature. These observations suggest that relatively slow  $\alpha$ -H/ $\beta$ -H exchange does occur at higher temperatures, presumably via species **VIa**. Unfortunately, thermal decomposition of **III** above 250 K complicated interpretations of the NMR experiments undertaken.

To further investigate the exchange processes, we therefore conducted an experiment utilizing a deuterated analogue of **I**, [Cp<sub>2</sub>Ti(CD<sub>3</sub>)(CD<sub>2</sub>Cl<sub>2</sub>)] [B(C<sub>6</sub>F<sub>5</sub>)<sub>4</sub>]. On reaction of **I-d<sub>3</sub>** with TMVS at 205 K, a <sup>1</sup>H NMR spectrum of the reaction mixture exhibited initially the expected Cp,  $\alpha$ -CH<sub>a</sub>,  $\alpha$ -CH<sub>b</sub>,  $\beta$ -CH, and SiMe<sub>3</sub> resonances peaks of **III-d<sub>3</sub>**, the relative Cp: $\alpha$ -CH<sub>2</sub>:SiMe<sub>3</sub>: $\beta$ -CH: $\beta$ -Me integrations being 10:2:9:1.1:~0. The temperature was raised to and held at 225 K for several hours, and the resonance of the  $\beta$ -Me group was observed to rise out of the baseline, indicating slow and at least partial replacement of deuterium by hydrogen atoms. Furthermore, as the broad resonance of the  $\beta$ -Me resonance grew in, the  $\alpha$ -CH<sub>a</sub>,  $\alpha$ -CH<sub>b</sub>, and  $\beta$ -CH resonances weakened proportionately while always maintaining essentially identical intensities.

The three resonances also retained their initial multiplet patterns, there being no evidence for the appearance of  $\alpha$ -CHD or  $\alpha$ -CH<sub>2</sub> doublets attributable to the presence of the isotopomers [Cp<sub>2</sub>TiCHDCH(CHD<sub>2</sub>)SiMe<sub>3</sub>]<sup>+</sup> or [Cp<sub>2</sub>TiCH<sub>2</sub>CD(CHD<sub>2</sub>)SiMe<sub>3</sub>]<sup>+</sup>, respectively, in the product. Assuming a normal deuterium isotope upfield shift of ~0.02 ppm,<sup>16</sup> the presence of [Cp<sub>2</sub>TiCHDCH(CHD<sub>2</sub>)SiMe<sub>3</sub>]<sup>+</sup> or [Cp<sub>2</sub>TiCH<sub>2</sub>CD(CHD<sub>2</sub>)SiMe<sub>3</sub>]<sup>+</sup> would have been apparent because of the appearance of new resonances and/or altering of the relative intensities of the components of the three multiplets. The redistribution reaction proceeded more rapidly at higher temperatures, e.g., 245 K, and was readily followed by <sup>2</sup>D NMR spectroscopy, which confirmed that  $\alpha$ -CD<sub>a</sub>,  $\alpha$ -CD<sub>b</sub>, and  $\beta$ -CD resonances increased in intensity at essentially equal rates during the reaction.

Interestingly, the Cp resonance of **III-d<sub>3</sub>** at  $\delta$  6.10 also weakened and a new Cp resonance at  $\delta$  6.05 grew in. The sum of the intensities of the two Cp resonances remained constant at 10H relative to the 9H intensity of the Me<sub>3</sub>Si resonance, for which no new resonance could be resolved, and thus, the reaction being monitored appears to be that shown in Scheme 5 rather than a process involving random replacement of  $\alpha$ - or  $\beta$ -H atoms.

The disappearance of [Cp<sub>2</sub>TiCH<sub>2</sub>CH(CD<sub>3</sub>)(SiMe<sub>3</sub>)]<sup>+</sup> and the apparent appearance of solely the isotopomeric product [Cp<sub>2</sub>TiCD<sub>2</sub>CD(CH<sub>3</sub>)(SiMe<sub>3</sub>)]<sup>+</sup> were monitored for 7 h at 225 K, and Figure 5 shows plots for the decrease with time of the

Scheme 5. Deuterium Redistribution in **III-d<sub>3</sub>**

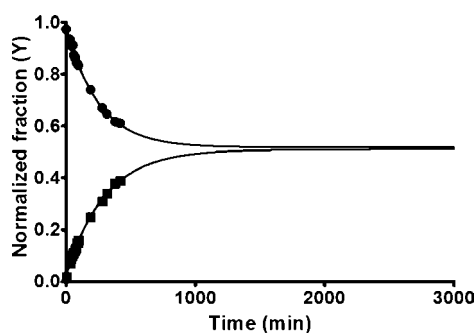
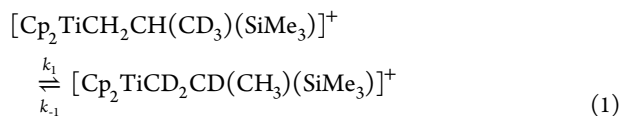


**Figure 5.** Plots showing the decrease in intensities of the resonances of  $[\text{Cp}_2\text{TiCH}_2\text{CH}(\text{CD}_3)(\text{SiMe}_3)]^+$  (upper) and the increase in intensity of the Cp resonance of  $[\text{Cp}_2\text{TiCD}_2\text{CD}(\text{CH}_3)(\text{SiMe}_3)]^+$  (lower) with time at 225 K.

integrated intensities of  $[\text{Cp}_2\text{TiCH}_2\text{CH}(\text{CD}_3)(\text{SiMe}_3)]^+$  (as the average of the intensities of the  $\alpha\text{-CH}_a$ ,  $\alpha\text{-CH}_b$ , and Cp resonances, normalized to the  $\text{Me}_3\text{Si}$  resonance as 9H), and for the concomitant increase with time of the Cp resonance at  $\delta$  6.05 of  $[\text{Cp}_2\text{TiCD}_2\text{CD}(\text{CH}_3)(\text{SiMe}_3)]^+$ .

As can be seen, loss of  $[\text{Cp}_2\text{TiCH}_2\text{CH}(\text{CD}_3)(\text{SiMe}_3)]^+$  and growth of  $[\text{Cp}_2\text{TiCD}_2\text{CD}(\text{CH}_3)(\text{SiMe}_3)]^+$  both appear to exhibit exponential behavior while the isotopic redistribution process clearly had not reached equilibrium within the 7 h over which the reaction was monitored. The data were therefore, using Prism software,<sup>17a</sup> treated as a reversible, first-order process (eq 1).<sup>17b</sup>



$$Y' = \frac{k_1 e^{-(k_1+k_{-1})(t+a)} + k_{-1}}{k_1 + k_{-1}} \quad (2)$$

$$Y'' = k_1 \frac{1 - e^{-(k_1+k_{-1})(t+a)}}{k_1 + k_{-1}} \quad (3)$$

Here,  $Y'$  and  $Y''$  represent the normalized fractions of  $[\text{Cp}_2\text{TiCH}_2\text{CH}(\text{CD}_3)(\text{SiMe}_3)]^+$  and  $[\text{Cp}_2\text{TiCD}_2\text{CD}(\text{CH}_3)(\text{SiMe}_3)]^+$ , respectively, as a function of time,  $t$ . From an iterative best fit analysis of the data for the former (eq 2), the forward and reverse rate constants,  $k_1$  and  $k_{-1}$ , were found to be  $(1.92 \pm 0.08) \times 10^{-3}$  and  $(2.1 \pm 0.2) \times 10^{-3} \text{ min}^{-1}$ , respectively, and hence the equilibrium constant  $K = 0.93 \pm 0.14$  ( $R^2 = 0.9958$ ). From a similar analysis of the data for the product (eq 3), the forward and reverse rate constants,  $k_1$  and  $k_{-1}$ , were found to be  $(1.70 \pm 0.07) \times 10^{-3}$  and  $(1.6 \pm 0.2) \times 10^{-3} \text{ min}^{-1}$ , respectively, and hence the equilibrium constant  $K = 1.04 \pm 0.17$  ( $R^2 = 0.9982$ ). Averaging the two values of  $K$ , one obtains an equilibrium constant  $K_{\text{eq}} = 0.99 \pm 0.15$ , which does not differ from unity by a statistically significant amount.

In chemical reactions involving equilibration of hydrogen and deuterium atoms among chemically nonequivalent sites, it has been well-established that the heavier isotope accumulates in those positions where the carbon–hydrogen bonds are strongest.<sup>18a–c</sup> This occurs because of reduction in vibrational energy (zero-point energy) when the heavier deuterium atom is substituted for the lighter hydrogen atom at a site with the highest bond stretching force constant. While calculations suggest that  $\text{III-d}_3$  prefers by 0.14 kcal/mol the isotopomeric

structure containing agostic  $\text{CH}_3$  rather than agostic  $\text{CD}_3$  interactions (see below), which would be consistent with this argument, the uncertainties in the experimental measurements of Figure 5 are such that we cannot conclude therefrom with certainty which  $\gamma$ -agostic structure is preferred.

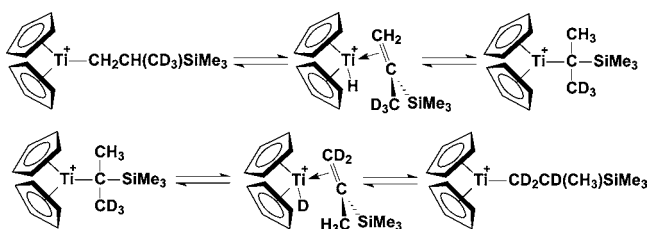
That said, the subtle but significant differences between the Cp resonances of **III** and its deuterated analogue seem to confirm that conversion from  $[\text{Cp}_2\text{TiCH}_2\text{CH}(\text{CD}_3)(\text{SiMe}_3)]^+$  to  $[\text{Cp}_2\text{TiCD}_2\text{CD}(\text{CH}_3)(\text{SiMe}_3)]^+$  (Scheme 5) results in a shift of the equilibrium (à la Scheme 2) toward the anticipated  $\gamma$ -H agostic isomer. Consistent with this, the temperature variation of the  $^1\text{H}$  NMR spectrum of **III**, in which the contribution of the  $\gamma$ -H agostic isomer to the averaged NMR parameters increases and that of the  $\beta$ -H agostic isomer decreases as the temperature decreases, shows that the Cp chemical shift of the  $\gamma$ -H agostic isomer lies at lower field than does the Cp resonance of the  $\beta$ -H agostic isomer ( $\delta$  6.07 at 215 K vs 6.14 at 250 K). Furthermore, as noted above, while  $^1J_{\text{CH}}$  for the  $\beta$ -H atom of **III** is 131, 133, and 137 Hz at 205, 225, and 250 K, respectively, that of  $[\text{Cp}_2\text{TiCH}_2\text{CH}(\text{CD}_3)(\text{SiMe}_3)]^+$  is 128 Hz at 225 K and 130 Hz at 250 K while  $^1J_{\text{CH}}$  of the methyl resonances of **III** and  $[\text{Cp}_2\text{TiCD}_2\text{CD}(\text{CH}_3)(\text{SiMe}_3)]^+$  at 250 K are  $\sim$ 133 and 126 Hz, respectively.

In the same vein, while deuteration of the  $\beta$ -methyl group results in essentially no change in the  $\alpha\text{-CH}_a$  and  $\alpha\text{-CH}_b$  chemical shifts ( $\Delta\delta \leq 0.01$  ppm) relative to those of **III-d**, the  $\beta$ -H resonance shifts upfield by  $\sim$ 0.07 ppm at 225 K, indicating a greater contribution of the  $\beta$ -agostic isomer to the (averaged)  $\beta$ -H chemical shift. Similarly, the  $\beta$ -Me ( $\gamma$ -H) resonance of  $[\text{Cp}_2\text{TiCD}_2\text{CD}(\text{CH}_3)(\text{SiMe}_3)]^+$  at 250 K is shifted upfield by  $\sim$ 0.08 ppm relative to that of **III-d**, suggesting an analogous shift to the  $\gamma$ -H agostic structure. Assuming that intrinsic chemical shifts change by  $-0.01$  ppm per vicinal D atom,<sup>16,18a–c</sup> we performed an analysis of the type discussed above for deducing equilibrium constants from comparisons of weighted-average observed with calculated  $\beta$ -H/ $\gamma$ -H chemical shifts. For purely  $\beta$ - and  $\gamma$ -agostic structures of the **III-d**<sub>3</sub> isotopomers at various temperatures, a difference in  $\Delta G$  value of  $\sim$ 0.12 kcal/mol was obtained for the  $\beta$ - and  $\gamma$ -agostic isomers of  $[\text{Cp}_2\text{TiCH}_2\text{CH}(\text{CD}_3)(\text{SiMe}_3)]^+$  at 225 K,<sup>18d</sup> in excellent agreement with the value of  $\sim$ 0.14 kcal/mol calculated between the  $\gamma$ -agostic isomers of  $[\text{Cp}_2\text{TiCH}_2\text{CH}(\text{CD}_3)(\text{SiMe}_3)]^+$  and  $[\text{Cp}_2\text{TiCD}_2\text{CD}(\text{CH}_3)(\text{SiMe}_3)]^+$  (see Supporting Information, Figure S16). Likewise, the free energy increase in the  $\beta$ -agostic conformation (in  $[\text{Cp}_2\text{TiCD}_2\text{CD}(\text{CH}_3)(\text{SiMe}_3)]^+$ ) due to  $\beta$ -deuteration is experimentally estimated at  $\sim$ 0.30 kcal/mol compared with a calculated value of  $\sim$ 0.29 kcal/mol (Supporting Information, Table S2).

In the case of  $[\text{Cp}_2\text{TiCD}_2\text{CD}(\text{CH}_3)(\text{SiMe}_3)]^+$ , in which random exchange between the  $\alpha\text{-CH}_a$ ,  $\alpha\text{-CH}_b$ , and  $\beta$ -H and the three  $\gamma$ -D atoms of the  $\beta$ - $\text{CD}_3$  group might seem possible, the deuterium atoms migrate from the methyl group to the other sites. Concurrently, because agostic bonding involving the  $\gamma$ -H atoms becomes more preferred relative to the newly formed  $\beta$ -agostic deuterium atom as the isotope redistribution proceeds, the position of the equilibrium of Scheme 2 changes such that  $K$  becomes larger. Similarly, during the isotopic redistribution shown in Scheme 5, the averaged Cp resonance of  $[\text{Cp}_2\text{TiCH}_2\text{CH}(\text{CD}_3)(\text{SiMe}_3)]^+$  ( $\delta$  6.10) is replaced by the averaged Cp resonance of  $[\text{Cp}_2\text{TiCD}_2\text{CD}(\text{CH}_3)(\text{SiMe}_3)]^+$  ( $\delta$  6.05), consistent with the  $\gamma$ -agostic isomer being more favored in the latter.

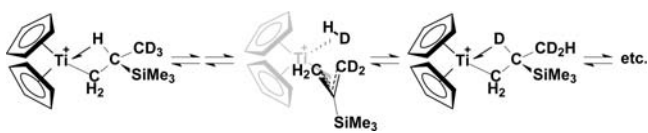
The deuterium rearrangement process, which is significantly slower than either the exchange shown in Scheme 2 or the  $\beta$ -H/ $\gamma$ -H exchange, could proceed via either or both of the mechanisms shown in Schemes 3 and 4. While the process shown in Scheme 3 cannot, for reasons discussed above, rationalize the low temperature  $\beta$ -H/ $\gamma$ -H exchange, high-temperature NOESY experiments indicate that relatively slow  $\alpha$ -H/ $\beta$ -H exchange does occur above  $\sim 250$  K, and therefore, the process shown in Scheme 3 may well be involved in deuterium redistribution. Indeed, it provides a better rationale for the slow, highly selective deuterium redistribution observed, as shown in Scheme 6.

**Scheme 6. Mechanism for Selective Isotope Redistribution**



In contrast, the allyl–dihydrogen mechanism of Scheme 4 seems less likely to be applicable to the isotope exchange because the presumed intermediacy of the HD–allyl species should result in a relatively random  $\beta$ -H/ $\gamma$ -H redistribution of deuterium isotopes during the higher temperature exchange process (Scheme 7).

**Scheme 7. Mechanism for Random Isotope H–D Redistribution**



There remains to be rationalized the fact that the low-temperature exchange process which involves the  $\beta$ -H atom and the three  $\gamma$ -H atoms of the  $\beta$ -methyl group but not the  $\alpha$ -CH<sub>2</sub> atoms of **III**-d<sub>0</sub>, revealed in EXSY experiments of **III**-d<sub>0</sub>, does not give rise to a corresponding process in **III**-d<sub>3</sub> which results in preferential redistribution of deuterium atoms to the  $\beta$ -CH position, we observe much slower redistribution of deuterium atoms to all of the  $\alpha$ -CH<sub>a</sub>,  $\alpha$ -CH<sub>b</sub>, and  $\beta$ -CH sites at comparable rates. In other words, while specific  $\beta$ -H/ $\gamma$ -H exchange is facile, specific  $\beta$ -H/ $\gamma$ -D exchange is not.

This observation seems to imply an unusually large kinetic isotope effect (KIE)<sup>19–22</sup> for the  $\beta$ -H/ $\gamma$ -H exchange process, much larger than the maximum primary KIE expected over the temperature range studied here (KIE 10–15) on the basis of zero-point energy differences and an “over-the-barrier” reaction involving C–H bond cleavage.<sup>19</sup> The KIE may be estimated by noting that the  $\beta$ -H/ $\gamma$ -H exchange happens within the approximate boundaries  $\sim 0.63$  Hz (from the mixing time in the EXSY experiment) < exchange rate < 6.9 Hz (the <sup>3</sup>J<sub>H(β)-H(γ)</sub> coupling constant observed at 250 K) in the temperature range 215–260 K, corresponding to a lifetime of  $\sim 1.6$  s. In direct contrast, as noted above for the process shown in Scheme 5, there was no evidence for the formation of [Cp<sub>2</sub>TiCH<sub>2</sub>CD-

(CHD<sub>2</sub>)SiMe<sub>3</sub>]<sup>+</sup> over 7 h (25 200 s) at 225 K, suggesting a KIE of >16 000 for  $\beta$ -H/ $\gamma$ -H exchange.

The only reasonable explanation that we see for this observation is a significant contribution of quantum mechanical tunnelling during the exchange process.<sup>19</sup> While the apparent KIE seems very large, the magnitude is not, in fact, without precedent.<sup>19c,d,21a–c</sup> Indeed, for previously studied examples of H(D) abstractions for which the KIEs are sufficiently large that deuterium abstraction does not occur, the term “all-or-nothing” isotope effect has been coined.<sup>19d</sup>

In addition to abnormally large H/D KIEs, tunnelling processes generally result also in reaction rates which are significantly higher than those anticipated on the basis of known (or calculated) thermal barriers; they also exhibit little temperature dependence.<sup>19,21</sup> As will be shown below in connection with Figure 7, the barrier to  $\beta$ -H/ $\gamma$ -H exchange is calculated to be  $\sim 16.5$  kcal/mol, which would result in reaction rates varying between  $6.5 \times 10^{-5}$  and  $2.0 \times 10^{-2}$  s<sup>-1</sup> in the temperature range 215–260 K,<sup>23a</sup> a factor of  $\sim 300$ ; this range is significantly higher than the maximum factor of  $\sim 12$  (6.9/0.63) found here. Furthermore, the rate of reaction found here at, e.g., 215 K,  $>0.63$  s<sup>-1</sup>, is far higher than the rate anticipated for a barrier of 16.5 kcal/mol.<sup>23a</sup>

Tunnelling of hydrogen atoms has occasionally been observed in organometallic and related systems,<sup>20</sup> an example being thermal rearrangement reactions of the cluster compounds M<sub>3</sub>(CO)<sub>10</sub>( $\mu$ -H)( $\mu$ -COH) (M = Ru, Os) to the dihydrides M<sub>3</sub>(CO)<sub>11</sub>H( $\mu$ -H). These reactions exhibit very large KIEs which are clearly manifested when the  $\mu$ -COH ligand is replaced by  $\mu$ -COD.<sup>20b,c</sup> A lower limit KIE of  $\sim 47$  was measured for the ruthenium compound but a much larger KIE was clearly operative in the case of the osmium analogue for which the rearrangement of the deuterated species was shut down completely, much as is observed here.

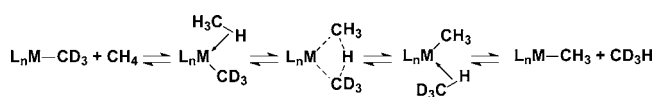
In a similar vein, albeit involving a very different type of chemistry, an apparently very large KIE is involved during the dissociative chemisorption of molecular hydrogen on a palladium surface.<sup>20d</sup> Whereas H<sub>2</sub> sorption at low temperatures results in H<sub>2</sub> dissociation and hydrogen atom combination with O atoms to form H<sub>2</sub>O, which is desorbed at higher temperatures, D<sub>2</sub> sorption results solely in D<sub>2</sub> desorption at higher temperatures. Thus, a KIE, which could not be measured, strongly suppresses D<sub>2</sub> dissociation and results in a significant alteration of the kinetic branching ratio in this system also. A process involving a deuterated species is again shut down completely. Thus, “all-or-nothing” isotope effects are well-established factors in organometallic and hydride chemistry.

Much closer to the chemistry involved in the  $\beta$ -H/ $\gamma$ -H exchange of **III**, quantum mechanical tunnelling is believed to be a major factor during methane  $\sigma$ -bond metathesis reactions with methyl compounds of the type Cp'<sub>2</sub>MCH<sub>3</sub> (Cp' = Cp or substituted Cp; M = Sc, Y, Lu), shown in eq 4.<sup>21</sup>



A number of mechanisms have been considered, with that shown in Scheme 8 having attracted considerable attention and being of probable relevance here.

Here a hydrogen moves reversibly from a  $\sigma$ -bonded CH<sub>4</sub> ligand, via a near linear C···H···C transition state (TS), to a –CD<sub>3</sub> group which becomes a  $\sigma$ -bonded CHD<sub>3</sub> ligand. Consideration of the charge distributions involved suggests that the reactions essentially involve proton transfer between pairs of methyl carbanions.<sup>21d</sup>

**Scheme 8. Mechanism for  $\sigma$ -Bond Metathesis of Methane and  $d^0/f$  Methyl Compounds**


Tunnelling has not been demonstrated explicitly for these reactions but was invoked because experimentally determined activation barriers were considerably lower (by up to  $\sim 12$  kcal/mol) than those predicted on the basis of DFT calculations.<sup>21a-c</sup> In addition, it was noted that the overall process involves considerable hydrogenic motion in the TS and thus may be expected to exhibit considerable light atom tunnelling behavior. KIEs of up to 3 orders of magnitude in the temperature range 300–400 K were estimated to account for the discrepancies in calculated and observed rate constants.<sup>21a-c</sup>

**Computational Studies of III.** Computational studies (DFT) were performed to obtain more insight into the agostic preference(s) of complex III and to rationalize the observed exchange processes. Total energies and free energies as well as structural drawings for all species considered are provided in the Supporting Information (Tables S1 and S2 and Figure S17).

The calculations yielded separate local minima corresponding to one  $\gamma$ -agostic, one  $\beta$ -agostic, and two  $\alpha$ -agostic structures, and in agreement with the experimental results, the  $\gamma$ -agostic structure was found to be lowest in free energy followed by the  $\beta$ -agostic structure (+1.9 kcal/mol), and the two  $\alpha$ -agostic structures were 3.0 and 4.2 kcal/mol higher than the  $\gamma$ -agostic structure. Transition states for interconversions between the various agostic species were located, and the network connecting them is summarized in Figure 6.

As can be seen, the methyl alkene intermediate complex of Scheme 1 and the barrier to insertion to form  $\gamma$ -agostic III lie at +13.6 and +18.9 kcal/mol, respectively. Thus, migratory insertion and deinsertion have barriers of 5.3 and 18.9 kcal/mol, respectively, and the insertion process of Scheme 1 is

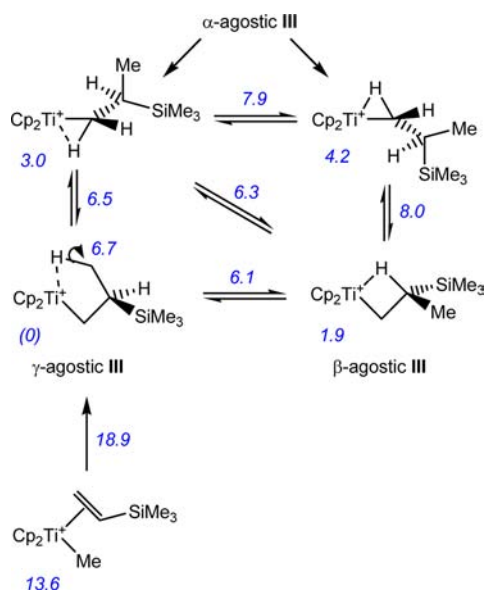


**Figure 6.** Calculated free energies of the agostic structures of III. Free energies (225 K) are in kcal/mol; energies at arrows correspond to transition states relative to  $\gamma$ -agostic III at zero.

therefore rapid and essentially irreversible once the TMVS complex has formed.

Three different paths were identified for exchange of  $\gamma$ -agostic III with its  $\alpha$ -agostic and  $\beta$ -agostic analogues: in-place methyl rotation, reversible conversion to the  $\beta$ -agostic structure, and reversible conversion to the more stable of the two  $\alpha$ -agostic structures. The calculated barriers for these three processes are essentially equal, 6.7, 6.1, and 6.5 kcal/mol, respectively, and agree well with the barrier for  $\gamma$ -H coalescence estimated from the  $^1\text{H}$  NMR data ( $\sim 7$  kcal/mol).<sup>23b</sup> The satisfyingly close agreement between calculated and experimental evidence lends credence to the appropriateness of our computational methodology.

The two different conventional hydrogen exchange paths of Schemes 3 and 4 were studied in detail and are summarized in Figure 7 for the all-H system III and in the Supporting Information (Figure S16) for the deuterated system III- $d_3$ .

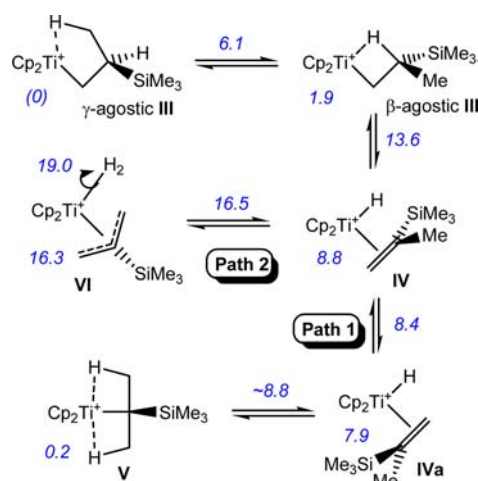


**Figure 7.** Calculated conventional paths for intramolecular hydrogen exchange in  $[\text{Cp}_2\text{TiCH}_2\text{CH}(\text{Me})(\text{SiMe}_3)]^+$ . Free energies (225 K) are in kcal/mol; energies at arrows correspond to transition states relative to  $\gamma$ -agostic III at zero.

As is shown, both paths begin with conventional  $\beta$ -hydrogen elimination which involves a transition state (TS) 13.6 kcal/mol above  $\gamma$ -agostic III. Path 1 (corresponding to Scheme 3) then continues with alkene rotation and reinsertion. These steps appear to be facile and to remain below the level of the original  $\beta$ -elimination TS. The free energy profile for alkene rotation in IV to rotamer IVa seems rather flat, and we could not locate a well-defined transition state for this step, but the highest point is calculated to be 8.4 kcal/mol above  $\gamma$ -agostic III. Rather surprisingly, the resulting tertiary alkyl insertion product V, which might be expected to be destabilized because of steric crowding, is in fact strongly stabilized by two  $\beta$ -agostic interactions and lies only 0.2 kcal/mol above  $\gamma$ -agostic III. Thus it seems likely that  $\beta$ -elimination of all of the six equivalent methyl hydrogens of V should be equally facile and would provide a mechanism for intramolecular hydrogen exchange between the  $\alpha$ -,  $\beta$ -, and  $\gamma$ -hydrogen atoms.

This path thus appears to provide an energetically feasible path for the observed H/D exchange between  $[\text{Cp}_2\text{TiCH}_2\text{CH}(\text{CD}_3)(\text{SiMe}_3)]^+$  and  $[\text{Cp}_2\text{TiCD}_2\text{CD}(\text{CH}_3)(\text{SiMe}_3)]^+$  (see the Supporting Information, Figure S16). There are significant isotope effects; for example, the conversion of  $\beta$ -agostic III to IV has a barrier of 13.6 kcal/mol, which becomes 13.7 kcal/mol

for its CD<sub>3</sub> deuterated isotopomer and 14.6 kcal/mol for the CD<sub>2</sub>CD isotopomer (much as anticipated<sup>20a</sup>). However, these differences of up to 1 kcal/mol would result in a KIE of up to ~5, i.e., far too little to correspond to the dramatic difference in behavior between **III** and **III-d<sub>3</sub>**. We also calculate a slight preference (~0.14 kcal/mol) for the  $\gamma$ -H over  $\gamma$ -D agostic structure, corresponding to a predicted population of 58:42 at equilibrium (225 K). This appears to be reasonably compatible with the results in Scheme 6, although, as mentioned above, it implies an equilibrium constant for eq 1 somewhat larger than that suggested by the data in Figure 5.

The alternative path 2 involves the allyl–dihydrogen species of Scheme 4 being formed from the same intermediate (hydride)(alkene) complex **IV** as in path 1. The mechanism shown in Figure 7 is the most reasonable conventional path we can think of that would rationalize our observation of  $\beta$ -H/ $\gamma$ -H exchange without the exchange involving also the  $\alpha$ -CH atoms. Furthermore, as we have noted above, this type of transformation enjoys substantial precedents.<sup>14</sup>

Indeed, Zhu and Ziegler have studied formation of allyl–dihydrogen complexes from sterically less encumbered alkenes,<sup>14f</sup> finding transition states for  $\beta$ -elimination and allyl formation steps at respectively ~8–16 and 10–14 kcal/mol above the  $\beta$ -agostic alkyl precursor (compared with our values of 13.6 and 16.5 kcal/mol, respectively). They also found that most allyl–dihydrogen complexes were only ~5–8 kcal/mol above the alkyl precursor but, not surprisingly, that steric hindrance strongly disfavors formation of the allyl–dihydrogen species. In this context, our system appears to fall in the “sterically hindered” category because of the SiMe<sub>3</sub> group, with allyl–dihydrogen complex formation endergonic by 16.3 kcal/mol. It follows that the relatively high energy path 2, involving  $\beta$ -H/ $\gamma$ -H exchange via the allyl–dihydrogen intermediate **VI**, would be preempted by the lower-energy path 1 involving doubly  $\beta$ -agostic insertion product **V**. The  $\beta$ -H/ $\gamma$ -H exchange should proceed at about the same rate as exchange with the  $\alpha$ -CH hydrogen atoms, which is not as indicated by the EXSY results, and exchange involving **III-d<sub>3</sub>** would, subject to any conventional KIEs, result in full deuterium scrambling at a rate comparable to the  $\beta$ -H/ $\gamma$ -H exchange. This also is not observed.

Instead all exchange involving the  $\alpha$ -CH hydrogen atoms is relatively slow and, for the conversion of [Cp<sub>2</sub>TiCH<sub>2</sub>CH(CD<sub>3</sub>)(SiMe<sub>3</sub>)]<sup>+</sup> to [Cp<sub>2</sub>TiCD<sub>2</sub>CD(CH<sub>3</sub>)(SiMe<sub>3</sub>)]<sup>+</sup> via species **V**, we estimate a barrier of 18 kcal/mol from the first-order rate constant  $k_1$  and the deuterium exchange data of Figure 5.<sup>23c</sup> This experimental barrier is significantly higher than the barrier calculated for the conversion of  $\beta$ -agostic **III** to **IV** (13.6 kcal/mol) and suggests a computationally unappreciated impediment to alkene rotation. While it is known that many DFT functionals underestimate barriers for hydrogen transfer reactions,<sup>24a</sup> the difference between calculated and observed barriers might also be due to external factors. For instance, the alkene rotation in **IV** to give **IVa**, a key step in path 1 of Figure 7, involves a significant geometric rearrangement and might well be hindered in solution by ion pair formation with the very bulky [B(C<sub>6</sub>F<sub>5</sub>)<sub>4</sub>]<sup>−</sup> counteranion. This factor was not taken into account in the isolated cationic species which we use in our computational model, and we note possible precedents for strong counteranion interactions impacting on internal molecular motions of metallocenium cations.<sup>24b</sup> In contrast, all other steps studied here result in relatively modest changes

in the overall shape of the cation and would hence be much less affected by the close presence of the counteranion.

However, if, in reality, alkene rotation in **IV** has for whatever reason a barrier of ~18 kcal/mol and is thus the rate-limiting step for any process involving **V** as an intermediate, then reactions involving the allyl–dihydrogen complex **VI** as an intermediate would be kinetically viable because of the lower barrier (16.5 kcal/mol). Path 2 would then be feasible as providing a mechanism for the observed  $\beta$ -H/ $\gamma$ -H exchange process, although we still have an apparent conundrum because it would remain unclear (a) why the calculated activation energy of ~16.5 kcal/mol above  $\gamma$ -agostic **III** is so much higher than the apparent activation energy for  $\beta$ -H/ $\gamma$ -H exchange determined on the basis of the rate of this reaction at 215 K (~12 kcal/mol; see above) and (b) why this path would not be available for the conversion of [Cp<sub>2</sub>TiCH<sub>2</sub>CH(CD<sub>3</sub>)(SiMe<sub>3</sub>)]<sup>+</sup> to specifically [Cp<sub>2</sub>TiCD<sub>2</sub>CD(CH<sub>3</sub>)(SiMe<sub>3</sub>)]<sup>+</sup>.

**Quantum Mechanical Proton Tunnelling?** In considering a tentative rationale, we have noted above that our experimental results seemingly require a sufficiently large KIE that quantum mechanical tunnelling must be operative at some point during the  $\beta$ -H/ $\gamma$ -H exchange process. In addition, as with the  $\sigma$ -bond metathesis reactions of Scheme 8, the experimentally determined activation barrier is significantly lower, by ~9 kcal/mol, than the calculated barrier. This again suggests quantum mechanical tunnelling.

For tunnelling to occur, the reaction coordinate must correspond to mostly hydrogen motion with little heavy-atom movement,<sup>19</sup> as in Scheme 8 for methane metathesis. In addition, the thermal barrier to hydrogen transfer must be high but narrow, with width comparable to the de Broglie wavelength of the hydrogen atom (1–2 Å)<sup>19a,b</sup> or, from a different perspective, comparable to the sum of the van der Waals radii<sup>25</sup> of the atoms concerned. The de Broglie wavelength, coupled with the substantial mass differences between the isotopes of hydrogen H and D, leads to sizable KIE values that greatly facilitate the investigation of tunneling processes. When dealing with reactions involving proton transfer over such distances, it is almost incumbent on one to consider tunnelling as being involved mechanistically.

The characteristics of reactions involving proton tunnelling have been subjected to very careful scrutiny in connection with a variety of enzymatically catalyzed processes<sup>21e,22</sup> for which H/D tunnelling is frequently characterized by unusually large KIEs. In such cases, proton transfer is considered to involve strongly hydrogen-bonded systems characterized by a double minimum potential with a medium-high barrier, as in Figure 8 which illustrates a system involving collinear proton transfer via tunnelling.<sup>21e,26</sup> As we show below, a similar double potential

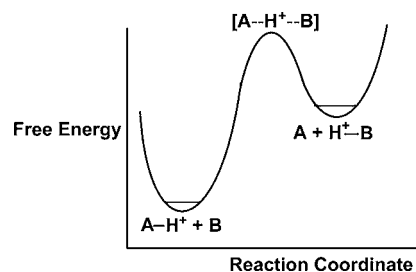


**Figure 8.** A double minimum free energy curve of type proposed for proton exchange in many enzymatic systems (A, B = C, N, O).

wall probably applies to the  $\beta$ -H/ $\gamma$ -H exchange under consideration here.

Although it was initially not clear to us just where tunnelling might be involved during  $\beta$ -H/ $\gamma$ -H exchange,  $\beta$ -hydrogen elimination/insertion reactions normally exhibit conventional KIEs<sup>20a</sup> and tunnelling is presumably not at play during the conversion of  $\beta$ -agostic **III** to **IV**. It therefore seems likely that the apparently very large KIE reflects tunnelling during exchange of the methyl hydrogen atoms and the hydride ligand of **IV**.

We have therefore investigated more closely the potential energy surface involved as **IV** isomerizes to the allyl-dihydrogen species **VI** as in Figure 7. The optimized structure of **IV** has a very asymmetric mode of coordination of the alkene to the titanium (Figure 9).

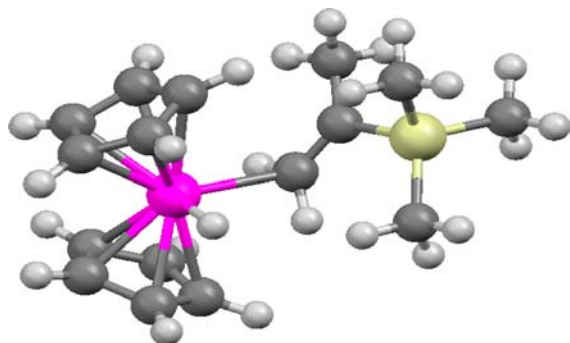


Figure 9. Structure of **IV**.

The structure of **IV** contains the expected bent Cp–Ti–Cp motif with the Ti–H and Ti–C(1) bonds lying essentially on the plane bisecting the Cp<sub>2</sub>Ti group. The hydride ligand lies at  $\sim 90^\circ$  to the C<sub>2</sub> axis of the Cp<sub>2</sub>Ti group, the Ti–H distance being 1.683 Å, while C(1) lies a few degrees off the C<sub>2</sub> axis. The Ti–C(1) and Ti–C(2) bond lengths are 2.42 and 3.40 Å, respectively, and while there are few relevant structural data available in the literature for comparisons, both are much longer than expected for Ti–C  $\sigma$  bonds and the Ti–C(1) bond length is comparable to Cp–Ti  $\pi$  bond lengths.<sup>27a</sup> The Ti–C(1)–C(2) bond angle is 125.4°, and thus the alkene is coordinated in an extremely asymmetric fashion.

The structure of **IV** is thus very similar to that of [Cp<sub>2</sub>Zr(Me)(DMP)]<sup>+</sup>, shown in Figure 1. Both exhibit very asymmetric coordination modes, induced apparently by the presence of two substituents on C(2). Indeed, presumably because of the smaller size of the titanium atom and the larger groups on C(2) of **IV**, the latter compound is more distorted from an  $\eta^2$  mode of coordination than is [Cp<sub>2</sub>Zr(Me)(DMP)]<sup>+</sup>. Interestingly, since rapid rotation of the R(Me)C= group along the C(1)–C(2) axis and relative to the =CH<sub>2</sub> group of [Cp<sub>2</sub>Zr(Me)(DMP)]<sup>+</sup> is observed,<sup>3</sup> rotation about the C(1)–C(2) bond of **IV** should also be facile. Thus, a requisite for  $\beta$ -H/ $\gamma$ -H exchange via tunneling, close mutual approach of the hydride ligand and a  $\gamma$ -hydrogen on the  $\beta$ -methyl group, is seemingly made possible by rotation about the Ti–C(1), C(1)–C(2), and C(2)–Me bonds.

As pointed out above, these structural features are consistent with the fact that 2,2-disubstituted 1-alkenes readily undergo carbocationic rather than coordination insertion polymerization.<sup>4</sup> Indeed, intermediates having the type of near  $\eta^1$  carbocationic structure shown in Figure 1 are believed to be

involved as end groups during carbocationic polymerization reactions of 2,2-disubstituted 1-alkenes.<sup>4</sup> The significant degree of positive charge results in the hydrogen atoms of such end groups being strongly acidic,<sup>4</sup> as indicated by the fact that chain transfer during, for example, carbocationic isobutene polymerization occurs via deprotonation of a chain end by the very weakly basic isobutene.<sup>4</sup> Thus, of great relevance here (see below), the  $\beta$ -methyl hydrogen atoms of **IV** should be strongly acidic.

Searching the energy profile linking **IV** and **VI**, we found a shallow local minimum, **VIII**, shown in Figure 10 and lying  $\sim 2.4$  kcal/mol above **IV**.

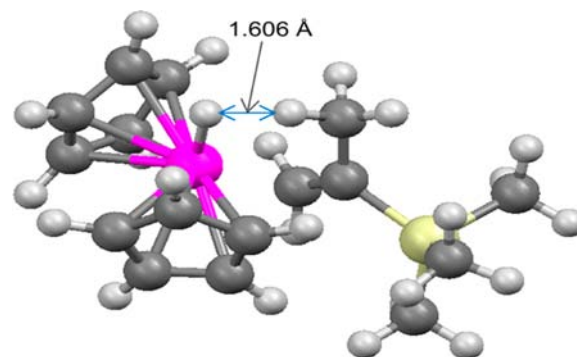


Figure 10. Structure of **VIII**.

In **VIII**, the Ti–H bond length is 1.685 Å, essentially unchanged from **IV**, while the Ti–C(1) and Ti–C(2) bond lengths are respectively 2.73 and 2.74 Å, marginally longer than the distance between the Ti and the carbon of the  $\beta$ -Me group, 2.72 Å. Thus, the three titanium–carbon distances in the incipient  $\eta^3$ -allylic titanium intermediate are nearly identical and, while longer than, e.g., the titanium–carbon distances in compounds of the type Cp<sub>2</sub>Ti( $\eta^3$ -allylic),<sup>27b</sup> they are significantly less than the sum of the van der Waals radii of carbon and titanium ( $\sim 3.9$  Å).<sup>25</sup>

In addition, we note the very close approach of a methyl hydrogen atom to the hydride ligand, the resulting H–H distance being 1.606 Å. This is considerably less than the sum of the van der Waals radii of  $\sim 2.18$ – $2.40$  Å for two hydrogen atoms<sup>25a</sup> and is probably a result of electrostatic attraction between the acidic  $\gamma$ -hydrogen (see above) and the negatively charged hydride.

This result is certainly consistent with the apparent involvement of quantum mechanical tunnelling during  $\beta$ -H/ $\gamma$ -H exchange, and in addition, the H(hydride)–H–C angle is nearly linear (166.3°). Thus, the system seems ideally set up to facilitate proton tunnelling of the type discussed above in connection with the exchange of Scheme 8 and that observed previously in enzymatically catalyzed processes.<sup>21e,22</sup>

We visualize a  $\sigma$ -bond metathesis-like process in which **VIII** (which appears to be thermally accessible from  $\gamma$ -agostic **III**) and a species similar to **VI** reside in potential wells much as in Figure 7, with **VIII** being the lower energy species. Transfer of a methyl hydrogen atom as a proton to the somewhat negatively charged hydride ligand to give a dihydrogen ligand would appear to be feasible and, given the dimensions of **VIII** (Figure 10), such a proton transfer must involve tunnelling. While the energy calculated for dihydrogen complex **VI** seems too high for it specifically to be capable of significant existence, in fact, the lifetime of the putative dihydrogen species need only

be sufficiently long that the dihydrogen ligand can assume an  $\eta^2$  structure in which the two hydrogen atoms are equivalent. Then both would have equal probability of transferring to the “allylic” carbon atom, and given that the methyl group undergoes free rotation, a tunnelling route to  $\beta$ -H/ $\gamma$ -H exchange is available.

Finally, we note that return of a proton from a dihydrogen ligand would be facilitated by the fact that dihydrogen ligands in cationic complexes are invariably strongly acidic.<sup>28</sup> Thus,  $\beta$ -H/ $\gamma$ -H exchange in **III** is rationalized on the basis of reversible tunnelling involving proton exchange between two acidic partners, much as in both methane  $\sigma$ -bond metathesis (Scheme 8) and several strongly hydrogen-bonded systems in enzymatically catalyzed processes.<sup>21e,22,26</sup>

## SUMMARY

The compound  $[\text{Cp}_2\text{Ti}(\text{Me})(\text{CD}_2\text{Cl}_2)][\text{B}(\text{C}_6\text{F}_5)_4]^+$  (**I**) reacts with trimethylvinylsilane (TMVS) to form the 1,2-insertion product  $[\text{Cp}_2\text{TiCH}_2\text{CHMe}(\text{SiMe}_3)]^+$  (**III**), which undergoes a most unusual array of exchange processes. Variable-temperature NMR studies show, for instance, that **III** exists as equilibrating  $\beta$ - and  $\gamma$ -agostic isomers with, surprisingly, the latter preferred by  $\sim 0.6$ – $1.9$  kcal/mol. In addition, while free rotation of the  $\beta$ -methyl group results in a single averaged  $\gamma$ -H atom resonance at higher temperatures, decoalescence occurs below  $\sim 200$  K, and the resonance of the  $\gamma$ -agostic H atom at  $\delta \sim -7.2$  can be observed. Free energy barriers to  $\beta$ -agostic/ $\gamma$ -agostic exchange and  $\gamma$ -H exchange (i.e., in-place  $\beta$ -methyl rotation) are both 6–7 kcal/mol. Reaction of  $[\text{Cp}_2\text{Ti}(\text{CD}_3)(\text{CD}_2\text{Cl}_2)]^+$  with TMVS resulted in the formation of  $[\text{Cp}_2\text{TiCH}_2\text{CH}(\text{CD}_3)(\text{SiMe}_3)]^+$ , which in turn converts slowly, via a reversible  $\beta$ -hydrogen elimination–reinsertion process, specifically to  $[\text{Cp}_2\text{TiCD}_2\text{CD}(\text{CH}_3)(\text{SiMe}_3)]^+$ . No other isotopomers were formed in this process, which has a barrier of  $\sim 18$  kcal/mol.

Finally, and most interesting of all, EXSY studies show that the  $\beta$ -H atom of **III** undergoes facile exchange with the three hydrogen atoms of the  $\beta$ -methyl group ( $\beta$ -H/ $\gamma$ -H exchange) but *not* with the two  $\alpha$ -H atoms. This exchange process is therefore very different from that involving deuterium atom redistribution and must also be associated with a very high kinetic isotope effect (KIE) because it is completely shut down when  $[\text{Cp}_2\text{TiCH}_2\text{CH}(\text{CD}_3)(\text{SiMe}_3)]^+$  is used. A reversible  $\beta$ -hydrogen elimination–reinsertion process does not seem to be involved in the  $\beta$ -H/ $\gamma$ -H exchange, but rather an allylic CH activation process similar to that posited previously to occur during metallocene-catalyzed propylene polymerization in order to account for the formation of dormant allylic species and the concomitant formation of  $\text{H}_2$  as a byproduct.<sup>1b,5f,14</sup> On the basis of an unusually large kinetic isotope effect and other factors, it is proposed that quantum mechanical proton tunnelling is involved during the  $\beta$ -H/ $\gamma$ -H exchange and, possibly, during allylic CH activation processes in general.

Complementing the variable-temperature NMR studies, DFT calculations were carried out to obtain energies and NMR parameters for all relevant structures and thence to obtain better insight into the agostic preference(s) of complex **III** and the observed exchange processes. NMR chemical shifts and coupling constants were also calculated, and in all cases where comparisons between experimental and calculated data were possible, agreement was excellent.

The ordering of stabilities of the agostic structures of **III**, observed and calculated, is different from those observed previously for  $[\text{Cp}_2\text{TiCH}_2\text{CHMeCH}_2\text{CHMe}_2]^+$  and

$[\text{Cp}_2\text{TiCH}_2\text{CH}_2\text{Bu}^t]^+$  ( $\beta$ -agostic preferred) and **II** ( $\alpha$ -agostic preferred).<sup>6e,f</sup> Judging from models, this is mainly a steric effect, a result of decreasing cone angles in the order  $\beta$ -Bu<sup>t</sup> >  $\beta$ -SiMe<sub>3</sub>  $\gg$   $\beta$ -H since, as noted elsewhere, an electronic preference for  $\beta$ -agostic structures generally holds true.<sup>5,6a–c,7</sup> However, a  $\beta$ -agostic structure forces the other two groups at a  $\beta$ -carbon atom to be in close contact with the Cp rings while, in contrast, crowding is a little less severe in the  $\gamma$ -agostic structure and is lowest in the  $\alpha$ -agostic structure of **II**, in which the distance between the  $\text{Cp}_2\text{Ti}$  fragment and the substituents is maximized. The extreme crowding in **II** therefore results in the  $\alpha$ -agostic structure being preferred, but the smaller cone angle of the Me<sub>3</sub>Si group compared with the Me<sub>3</sub>C group results in less crowding near the metal center for **III** with the result that this compound prefers the  $\gamma$ -agostic structure by a small margin. Reducing the size of the  $\beta$ -substituents even more leads to the “normal”  $\beta$ -agostic structures observed for  $[\text{Cp}_2\text{TiCH}_2\text{CHMeCH}_2\text{CHMe}_2]^+$  and  $[\text{Cp}_2\text{TiCH}_2\text{CH}_2\text{Bu}^t]^+$ .

## ASSOCIATED CONTENT

### Supporting Information

Figures and tables describing and elaborating on the NMR experiments; calculated energies for the  $\text{Cp}_2\text{TiCH}_3^+ + \text{VTMS}$  and  $\text{Cp}_2\text{TiCD}_3^+ + \text{VTMS}$  systems; calculated NMR parameters; b-p geometries, relative free energies and barriers, and calculated structures. This material is available free of charge via the Internet at <http://pubs.acs.org>.

## AUTHOR INFORMATION

### Corresponding Author

bairdmc@chem.queensu.ca

### Notes

The authors declare no competing financial interest.

## ACKNOWLEDGMENTS

M.C.B. gratefully acknowledges the Natural Science and Engineering Research Council of Canada and Queen's University for funding of this research. PHMB thanks the Natural Science and Engineering Research Council of Canada, the Canada Foundation for Innovation, the Manitoba Research and Innovation Fund, and SABIC Petrochemicals Europe for financial support. We thank Dr. Alexei Neverov and Mr. Mark Raycroft for assistance running GraphPad Software Prism, and A.D.-B. thanks Queen's University for a Carrel Graduate Fellowship.

## REFERENCES

- (1) For useful reviews, see the following: (a) Bochmann, M. J. *Chem. Soc., Dalton Trans.* **1996**, 255. (b) Resconi, L.; Camurati, I.; Sudmeijrt, O. *Top. Catal.* **1999**, 7, 145. (c) Coates, G. W. *Chem. Rev.* **2000**, 100, 1223. (d) Resconi, L.; Cavallo, L.; Fait, A.; Piemontesi, F. *Chem. Rev.* **2000**, 100, 1253. (e) Chen, E. Y.-X.; Marks, T. J. *Chem. Rev.* **2000**, 100, 1391. (f) Rappé, A. K.; Skiff, W. M.; Casewit, C. J. *Chem. Rev.* **2000**, 100, 1435. (g) Bochmann, M. J. *Organomet. Chem.* **2004**, 689, 3982. (h) Fujita, T.; Makio, H. *Comprehensive Organometallic Chemistry III*; Crabtree, R. H., Mingos, D. M. P., Eds.; Elsevier: Amsterdam, 2007; Chapter 11.20. (i) Froese, R. D. J. In *Computational Modeling for Homogeneous and Enzymatic Catalysis*; Morokuma, K., Musaev, D. G., Eds.; Wiley-VCH: Weinheim, Germany, 2008; p 149. (j) Busico, V. *Macromol. Chem. Phys.* **2007**, 208, 26. (k) Wilson, P. A.; Hannant, M. H.; Wright, J. A.; Cannon, R. D.; Bochmann, M. *Macromol. Symp.* **2006**, 236 (Olefin Polymerization), 100. (l) Alt, H. G.; Licht, E. H.; Licht, A. I.; Schneider, K. J. *Coord. Chem. Rev.* **2006**, 250, 2.

- (2) (a) Casey, C. P.; Carpenetti, D. W. *Organometallics* **2000**, *19*, 3970. (b) Carpentier, J. F.; Wu, Z.; Lee, C. W.; Strömberg, S.; Christopher, J. N.; Jordan, R. F. *J. Am. Chem. Soc.* **2000**, *122*, 7750 and references therein. (c) Brandow, C. G.; Mendiratta, A.; Bercaw, J. E. *Organometallics* **2001**, *20*, 4253. (d) Casey, C. P.; Carpenetti, D. W.; Sakurai, H. *Organometallics* **2001**, *20*, 4262. (e) Stoebenau, E. J.; Jordan, R. F. *J. Am. Chem. Soc.* **2006**, *128*, 8162. (f) Stoebenau, E. J.; Jordan, R. F. *J. Am. Chem. Soc.* **2006**, *128*, 8638.
- (3) (a) Vatamanu, M.; Stojcevic, G.; Baird, M. C. *J. Am. Chem. Soc.* **2008**, *130*, 454. (b) Sauriol, F.; Wong, E.; Leung, A. M. H.; Elliott Donaghue, I.; Baird, M. C.; Wondimagegn, T.; Ziegler, T. *Angew. Chem., Int. Ed.* **2009**, *48*, 3342.
- (4) Baird, M. C. *Chem. Rev.* **2000**, *100*, 1471.
- (5) For reviews of agostic complexes, see the following: (a) Brookhart, M.; Green, M. L. H. *J. Organomet. Chem.* **1983**, *250*, 395. (b) Brookhart, M.; Green, M. L. H.; Wong, L.-L. *Prog. Inorg. Chem.* **1988**, *36*, 1. (c) Grubbs, R. H.; Coates, G. W. *Acc. Chem. Res.* **1996**, *29*, 85. (d) Scherer, W.; McGrady, G. S. *Chem.—Eur. J.* **2003**, *9*, 6057. (e) Clot, E.; Eisenstein, O. *Struct. Bonding (Berlin)* **2004**, *113*, 1. (f) Scherer, W.; McGrady, G. S. *Angew. Chem., Int. Ed.* **2004**, *43*, 1782. (g) Brookhart, M.; Green, M. L. H.; Parkin, G. *Proc. Natl. Acad. Sci. U. S. A.* **2007**, *104*, 6908. (h) Lein, M. *Coord. Chem. Rev.* **2009**, *253*, 625. For computational papers discussing the importance of  $\beta$ -agostic structures during metallocene-induced alkene polymerization, see the following: (i) Lohrenz, J. C. W.; Woo, T. K.; Ziegler, T. *J. Am. Chem. Soc.* **1995**, *117*, 12793. (j) Jensen, V. R.; Koley, D.; Jagadeesh, M. N.; Thiel, W. *Macromolecules* **2005**, *38*, 10266. (k) Mitoraj, M. P.; Michalak, A.; Ziegler, T. *Organometallics* **2009**, *28*, 3727. (l) Scherer, W.; Herz, V.; Hauf, C. *Struct. Bonding (Berlin)* **2012**, *146*, 159. (m) Laine, A.; Linnolahti, M.; Pakkanen, T. A.; Severn, J. R.; Kokko, E.; Pakkanen, A. *Organometallics* **2010**, *29*, 1541. (n) Laine, A.; Linnolahti, M.; Pakkanen, T. A.; Severn, J. R.; Kokko, E.; Pakkanen, A. *Organometallics* **2011**, *30*, 1350. (o) Dawoodi, Z.; Green, M. L. H.; Mtetwa, V.; Prout, K.; Schultz, A. J.; Williams, J. M.; Koetzel, T. F. *J. Chem. Soc., Dalton Trans.* **1986**, 1629. (p) Scherer, W.; Priermeier, T.; Haaland, A.; Volden, H. V.; McGrady, G. S.; Downs, A. J.; Boese, R.; Bläser, D. *Organometallics* **1998**, *17*, 4406. For papers describing specifically late transition metal agostic complexes, see the following: (q) Brookhart, M.; Lincoln, D. M.; Volpe, A. F.; Schmidt, G. F. *Organometallics* **1989**, *8*, 1212. (r) Shultz, L. H.; Brookhart, M. *Organometallics* **2001**, *20*, 3975.
- (6) (a) Jordan, R. F.; Bradley, P. K.; Baenziger, N. C.; Lapointe, R. E. *J. Am. Chem. Soc.* **1990**, *112*, 1289. (b) Alelyunas, Y. W.; Guo, Z.; Lapointe, R. E.; Jordan, R. F. *Organometallics* **1993**, *12*, 544. (c) Alelyunas, Y. W.; Baenziger, N. C.; Bradley, P. K.; Jordan, R. F. *Organometallics* **1994**, *13*, 148. (d) Guo, Z.; Swenson, D. C.; Jordan, R. F. *Organometallics* **1994**, *13*, 1424. (e) Sauriol, F.; Sonnenberg, J. F.; Chadder, S. J.; Dunlop-Brière, A. F.; Baird, M. C.; Budzelaar, P. H. M. *J. Am. Chem. Soc.* **2010**, *132*, 13357. (f) Dunlop-Brière, A. F.; Baird, M. C.; Budzelaar, P. H. M. *Organometallics* **2012**, *31*, 1591.
- (7) A number of computational papers consider the interplay between  $\alpha$ - and  $\beta$ -agostic species; see the following: (a) Nifant'ev, I. E.; Ustynyuk, L. Y.; Laikov, D. N. *Organometallics* **2001**, *20*, 5375. (b) Graf, M.; Angermund, K.; Fink, G.; Thiel, W.; Jensen, V. R. *J. Organomet. Chem.* **2006**, *691*, 4367. (c) Karttunen, V. A.; Linnolahti, M.; Pakkanen, T. A.; Severn, J. R.; Kokko, E.; Maaranen, J.; Pitkänen, P. *Organometallics* **2008**, *27*, 3390.
- (8) TMVS is polymerized via anionic initiation; see the following: (a) Rickle, G. K. *J. Macromol. Sci.-Chem.* **1986**, *A23*, 1287. (b) Oku, J.-I.; Hasegawa, T.; Takeuchi, T.; Takai, M. *Polym. J.* **1991**, *23*, 1377. (c) Gan, Y.; Prakash, S.; Olah, G. A.; Weber, W. P.; Hogen-Esch, T. E. *Macromolecules* **1996**, *26*, 8285. (d) Rangou, S.; Shishatskiy, S.; Filiz, V.; Abetz, V. *Eur. Polym. J.* **2011**, *47*, 723.
- (9) For examples, see the following: (a) Peng, T.-S.; Arif, A. M.; Gladysz, J. A. *Helv. Chim. Acta* **1992**, *75*, 442. (b) Lenges, C. P.; White, P. S.; Brookhart, M. *J. Am. Chem. Soc.* **1998**, *120*, 6965. (c) Böhm, V. P. W.; Brookhart, M. *Angew. Chem., Int. Ed.* **2001**, *40*, 4694. (d) Hapke, M.; Weding, N.; Spannenberg, A. *Organometallics* **2010**, *29*, 4298. (e) Lipponen, S. H.; Seppälä, J. V. *Organometallics* **2011**, *30*, 528.
- (10) (a) Ahlrichs, R.; Armbruster, M. K.; Bachorz, R. A.; Bär, M.; Baron, H.-P.; Bauernschmitt, R.; Bischoff, F. A.; Böcker, S.; Crawford, N.; Deglmann, P.; Della Sala, F.; Diedenhofen, M.; Ehrig, M.; Eichkorn, K.; Elliott, S.; Friese, D.; Furche, F.; Glöss, A.; Haase, F.; Häser, M.; Hättig, C.; Hellweg, A.; Höfener, S.; Horn, H.; Huber, C.; Huniar, U.; Kattannek, M.; Klopper, W.; Köhn, A.; Kölmel, C.; Kollwitz, M.; May, K.; Nava, P.; Ochsenfeld, C.; Öhm, H.; Pabst, M.; Patzelt, H.; Rappoport, D.; Rubner, O.; Schäfer, A.; Schneider, U.; Sierka, M.; Tew, D. P.; Treutler, O.; Unterreiner, B.; von Arnim, M.; Weigend, F.; Weis, P.; Weiss, H.; Winter, N. *Turbomole Version 5*; Theoretical Chemistry Group, University of Karlsruhe, 2002. (b) Treutler, O.; Ahlrichs, R. *J. Chem. Phys.* **1995**, *102*, 346. (c) Schäfer, A.; Huber, C.; Ahlrichs, R. *J. Chem. Phys.* **1994**, *100*, 5829. (d) Becke, A. D. *Phys. Rev. A* **1988**, *38*, 3098. (e) Perdew, J. P. *Phys. Rev. B* **1986**, *33*, 8822. (f) All Turbomole calculations were performed with the functionals “b-p” and “b3-lyp” of that package, which are similar (but not identical) to the Gaussian “BP86” and “B3LYP” functionals. (g) Lee, C.; Yang, W.; Parr, R. G. *Phys. Rev. B* **1988**, *37*, 785. (h) Becke, A. D. *J. Chem. Phys.* **1993**, *98*, 1372. (i) Becke, A. D. *J. Chem. Phys.* **1993**, *98*, 5648. (j) PQS version 2.4; Parallel Quantum Solutions: Fayetteville, AR, 2001 (the Baker optimizer is available separately from PQS upon request). (k) Baker, J. *J. Comput. Chem.* **1986**, *7*, 385. (l) Stephens, P. J.; Devlin, F. J.; Chabalowski, C. F.; Frisch, M. J. *J. Phys. Chem.* **1994**, *98*, 11623. (m) McWeeny, R. *Phys. Rev.* **1962**, *126*, 1028. (n) Ditchfield, R. *Mol. Phys.* **1974**, *27*, 789. (o) Dodds, J. L.; McWeeny, R.; Sadlej, A. J. *Mol. Phys.* **1980**, *41*, 1419. (p) Wolinski, K.; Hilton, J. F.; Pulay, P. *J. Am. Chem. Soc.* **1990**, *112*, 8251. (q) Helgaker, T.; Watson, M.; Handy, N. C. *J. Chem. Phys.* **2000**, *113*, 9402. (r) Sychrovsky, V.; Grafenstein, J.; Cremer, D. *J. Chem. Phys.* **2000**, *113*, 3530. (s) Barone, V.; Peralta, J. E.; Contreras, R. H.; Snyder, J. P. *J. Phys. Chem. A* **2002**, *106*, 5607. (t) Peralta, J. E.; Contreras, R. H.; Cheeseman, J. R.; Frisch, M. J.; Scuseria, G. E. *Chem. Phys. Lett.* **2003**, *375*, 452.
- (11) (a) Weigend, F.; Furche, F.; Ahlrichs, R. *J. Chem. Phys.* **2003**, *119*, 12753. (b) Klamt, A.; Schürmann, G. *J. Chem. Soc. Perkin Trans. 2* **1993**, *5*, 799. (c) Tobisch, S.; Ziegler, T. *J. Am. Chem. Soc.* **2004**, *126*, 9059. (d) Raucoles, R.; De Bruin, T.; Raybaud, P.; Adamo, C. *Organometallics* **2009**, *28*, 5358. (e) Frisch, M. J.; Trucks, G. W.; Schlegel, H. B.; Scuseria, G. E.; Robb, M. A.; Cheeseman, J. R.; Montgomery, J. A., Jr.; Vreven, T.; Kudin, K. N.; Burant, J. C.; Millam, J. M.; Iyengar, S. S.; Tomasi, J.; Barone, V.; Mennucci, B.; Cossi, M.; Scalmani, G.; Rega, N.; Petersson, G. A.; Nakatsuji, H.; Hada, M.; Ehara, M.; Toyota, K.; Fukuda, R.; Hasegawa, J.; Ishida, M.; Nakajima, T.; Honda, Y.; Kitao, O.; Nakai, H.; Klene, M.; Li, X.; Knox, J. E.; Hratchian, H. P.; Cross, J. B.; Bakken, V.; Adamo, C.; Jaramillo, J.; Gomperts, R.; Stratmann, R. E.; Yazyev, O.; Austin, A. J.; Cammi, R.; Pomelli, C.; Ochterski, J. W.; Ayala, P. Y.; Morokuma, K.; Voth, G. A.; Salvador, P.; Dannenberg, J. J.; Zakrzewski, V. G.; Dapprich, S.; Daniels, A. D.; Strain, M. C.; Farkas, O.; Malick, D. K.; Rabuck, A. D.; Raghavachari, K.; Foresman, J. B.; Ortiz, J. V.; Cui, Q.; Baboul, A. G.; Clifford, S.; Cioslowski, J.; Stefanov, B. B.; Liu, G.; Liashenko, A.; Piskorz, P.; Komaromi, I.; Martin, R. L.; Fox, D. J.; Keith, T.; Al-Laham, M. A.; Peng, C. Y.; Nanayakkara, A.; Challacombe, M.; Gill, P. M. W.; Johnson, B.; Chen, W.; Wong, M. W.; Gonzalez, C.; Pople, J. A. *Gaussian 03, Revision C.02*; Gaussian, Inc.: Wallingford, CT, 2004. (f) Kutzelnigg, W.; Fleischer, U.; Schindler, M. The IGLO-Method: Ab Initio Calculation and Interpretation of NMR Chemical Shifts and Magnetic Susceptibilities. In *NMR Basic Principles and Progress*; Diehl, P.; Flück, E.; Günther, H.; Kosfeld, R.; Seelig, J., Eds.; Springer-Verlag: Heidelberg, 1990; Vol. 23.
- (12) (a) Papajak, E.; Leverentz, H. R.; Zheng, J.; Truhlar, D. G. *J. Chem. Theory Comput.* **2009**, *5*, 1197. (b) Papajak, E.; Truhlar, D. G. *J. Chem. Theory Comput.* **2010**, *6*, 597. (c) Dunning, T. H. *J. Chem. Phys.* **1989**, *90*, 1007. (d) Kendall, R. A.; Dunning, T. H.; Harrison, R. J. *J. Chem. Phys.* **1992**, *96*, 6796. (e) Woon, D. E.; Dunning, T. H. *J. Chem. Phys.* **1993**, *98*, 1358. (f) Dunning, T. H.; Peterson, K. A.; Wilson, A.

K. *J. Chem. Phys.* **2001**, *114*, 9244. (g) Balabanov, N. B.; Peterson, K. A. *J. Chem. Phys.* **2005**, *123*, 064107.

(13) (a) Feller, D. *J. Comput. Chem.* **1996**, *17*, 1571. (b) Schuchardt, K. L.; Didier, B. T.; Elsethagen, T.; Sun, L.; Gurumoorathi, V.; Chase, J.; Li, J.; Windus, T. L. *J. Chem. Inf. Model.* **2007**, *47*, 1045.

(14) (a) Margl, P. M.; Woo, T. K.; Blöchl, P. E.; Ziegler, T. *J. Am. Chem. Soc.* **1998**, *120*, 2174. (b) Margl, P. M.; Woo, T. K.; Ziegler, T. *Organometallics* **1998**, *17*, 4997. (c) Resconi, L. *J. Mol. Catal., A* **1999**, *146*, 167. (d) Longo, P.; Grisi, F.; Guerra, G.; Cavallo, L. *Macromolecules* **2000**, *33*, 4647. (e) Moscardi, M.; Resconi, L.; Cavallo, L. *Organometallics* **2001**, *20*, 1918. (f) Zhu, C.; Ziegler, T. *Inorg. Chim. Acta* **2003**, *345*, 1. (g) Pilme, J.; Busico, V.; Cossi, M.; Talarico, G. *J. Organomet. Chem.* **2007**, *692*, 4227.

(15) (a) Lauher, J. W.; Hoffmann, R. *J. Am. Chem. Soc.* **1976**, *98*, 1729. (b) Albricht, T. A.; Burdett, J. K.; Whangbo, M.-H. *Orbital Interactions in Chemistry*; Wiley: New York, 1985; p 393.

(16) For relevant reviews on the influence of isotope effects on chemical shifts, see the following: (a) Batiz-Hernandez, H.; Bernheim, R. A. *Prog. NMR Spectrosc.* **1967**, *3*, 63. (b) Hansen, P. E. *Annu. Rep. NMR Spectrosc.* **1983**, *15*, 105.

(17) (a) *GraphPad Software Prism, Version 3.02*. The  $a$  parameters in each equation are the calculated offsets from the initial starting times of the reactions, since each had already started prior to the first acquisition point. The values obtained by iteration are  $9.9 \pm 3.8$  min for  $Y'$  and  $15.2 \pm 2.9$  min for  $Y''$ . (b) Espenson, J. H. *Chemical Kinetics and Reaction Mechanisms*; McGraw-Hill: New York, 1981; p 42. (c) Espenson, J. H. *Chemical Kinetics and Reaction Mechanisms*; McGraw-Hill: New York, 1981; Chapter 6.

(18) For relevant reviews on the influence of isotope effects on chemical equilibria, see the following: (a) Jameson, C. J. *Isotopes in Physical and Biomedical Science*; Buncl, E., Jones, J. R., Eds.; Elsevier: New York, 1991; Vol. 2, p 1. (b) Jameson, C. J. *Encycl. Nucl. Magn. Reson.* **1996**, *4*, 2638. (c) Jankowski, S. *Annu. Rep. NMR Spectrosc.* **2009**, *68*, 149. (d) Experimental values obtained from linear regressions of  $\Delta G = \Delta H - T\Delta S$  (from equilibrium constants) against temperature, where  $\Delta H$  is the enthalpy difference between  $\gamma$ - and  $\beta$ -agostic conformations  $\{-1.40 \pm 0.04$  kcal/mol for  $[\text{Cp}_2\text{TiCH}_2\text{CH}(\text{CD}_3)(\text{SiMe}_3)]^+$  and  $-2.69 \pm 0.03$  kcal/mol for  $[\text{Cp}_2\text{TiCD}_2\text{CD}(\text{CH}_3)(\text{SiMe}_3)]^+$  and  $\Delta S$  is the analogous entropy difference  $\{-4.2 \pm 0.1$  cal/(mol·K) for  $[\text{Cp}_2\text{TiCH}_2\text{CH}(\text{CD}_3)(\text{SiMe}_3)]^+$  and  $-8.0 \pm 0.1$  cal/(mol·K) for  $[\text{Cp}_2\text{TiCD}_2\text{CD}(\text{CH}_3)(\text{SiMe}_3)]^+$  with  $R^2$  of 0.9934 and 0.9991 and  $\Delta G_{\beta \rightarrow \gamma\text{-agostic}}$  at 225 K of  $-0.46$  and  $-0.89$  kcal/mol, respectively}. These  $\Delta(\Delta G_{\beta \rightarrow \gamma\text{-agostic}})$  experimental and calculated values correspond to a change in the  $\beta$ -agostic/ $\gamma$ -agostic contribution ratio by a factor of  $\sim 0.39$  and of  $\sim 0.37$  (225 K), respectively, going from  $[\text{Cp}_2\text{TiCH}_2\text{CH}(\text{CD}_3)(\text{SiMe}_3)]^+$  to  $[\text{Cp}_2\text{TiCD}_2\text{CD}(\text{CH}_3)(\text{SiMe}_3)]^+$ , consistent with the significant difference observed in their respective Cp chemical shifts. Assuming that the changes in  $\Delta G_{\beta \rightarrow \gamma\text{-agostic}}$  of **III-d**<sub>3</sub> relative to that of **III-d**<sub>0</sub> originate primarily from the increase in free energy of the D-agostic conformer of question, we obtain a 0.12 kcal/mol experimental increase in free energy of the  $\gamma$ -D-agostic conformation at 225 K, in very close agreement with the computed 0.14 kcal/mol discussed above. Likewise, the free energy increase in the  $\beta$ -agostic conformation due to  $\beta$ -deuteration is experimentally estimated at 0.30 kcal/mol, calculated to be 0.29 kcal/mol (see the Supporting Information, Table S2).

(19) For background theory on KIEs, see the following: (a) Caldin, E. F. *Chem. Rev.* **1969**, *69*, 135. (b) Bell, R. P. *Chem. Soc. Rev.* **1974**, *3*, 513. (c) More O'Ferrall, R. A. *J. Phys. Org. Chem.* **2010**, *23*, 572. For examples of very large KIEs, see the following: (d) Wang, J.-T.; Williams, F. J. *Am. Chem. Soc.* **1972**, *94*, 2930. (e) Brunton, G.; Griller, D.; Barclay, L. R. C.; Ingold, K. U. *J. Am. Chem. Soc.* **1976**, *98*, 6803.

(20) (a) For a recent, highly relevant and useful review of KIEs in organometallic chemistry, see the following: Gómez-Gallego, M.; Sierra, M. A. *Chem. Rev.* **2011**, *111*, 4857 and references therein. (b) Pribich, D. C.; Rosenberg, E. *Organometallics* **1988**, *7*, 1741. (c) Hash, K. R.; Field, R. J.; Rosenberg, E. *Inorg. Chim. Acta* **1997**, *259*,

329. (d) Hakanoglu, C.; Hawkins, J. M.; Asthagiri, A.; Weaver, J. F. *J. Phys. Chem. C* **2010**, *114*, 11485.

(21) (a) Sherer, E. C.; Cramer, C. J. *Organometallics* **2003**, *22*, 1682. (b) Woodrum, N. L.; Cramer, C. J. *Organometallics* **2006**, *25*, 68. (c) Lewin, J. L.; Woodrum, N. L.; Cramer, C. J. *Organometallics* **2006**, *25*, 5906. (d) Barros, N.; Eisenstein, O.; Maron, L. *Dalton Trans.* **2006**, 3052. For a recent review of computational research on C–H activation by transition metal complexes, see the following: (e) Balcells, D.; Clot, E.; Eisenstein, O. *Chem. Rev.* **2010**, *110*, 749.

(22) See, for instance, the following: (a) Mielke, Z.; Sobczyk, L. In *Isotope Effects in Chemistry and Biology*; Kohen, A., Limbach, H.-H., Eds.; Taylor & Francis: New York, 2006; p 281. (b) Smedarchina, Z.; Siebrand, W.; Fernández-Ramos, A. In *Isotope Effects in Chemistry and Biology*; Kohen, A., Limbach, H.-H., Eds.; Taylor & Francis: New York, 2006; p 521. (c) Kiefer, P. M.; Hynes, J. T. In *Isotope Effects in Chemistry and Biology*; Kohen, A., Limbach, H.-H., Eds.; Taylor & Francis: New York, 2006; p 549. (d) Siebrand, W.; Smedarchina, Z. In *Isotope Effects in Chemistry and Biology*; Kohen, A., Limbach, H.-H., Eds.; Taylor & Francis: New York, 2006; p 725. (e) Limbach, H.-H.; Lopez, J. M.; Kohen, A. *Philos. Trans. R. Soc. B* **2006**, *361*, 1399.

(23) (a) Estimated on the basis of the standard expression  $k = (k_B T/h) \exp(-\Delta G/RT)$ .<sup>22e</sup> (b) Estimated by simulation of an exchange spectrum based on Figures 1 and 2 and using the expression  $k = (k_B T/h) \exp(-\Delta G/RT)$ . The error margin is probably  $\sim 1$  kcal/mol. (c) Estimated by simulations utilizing the data of Figure 5 and the expression  $k = (k_B T/h) \exp(-\Delta G/RT)$ . The error margin is probably  $\sim 1$  kcal/mol.

(24) (a) Talarico, G.; Blok, A. N. J.; Woo, T. K.; Cavallo, L. *Organometallics* **2002**, *21*, 4939 and references therein. (b) Busico, V.; Van Axel Castelli, V.; Aprea, P.; Cipullo, R.; Segre, A.; Talarico, G.; Vacatello, M. *J. Am. Chem. Soc.* **2003**, *125*, 5451.

(25) (a) Rowland, R. S.; Taylor, R. J. *Phys. Chem.* **1996**, *100*, 7384. (b) Nag, S.; Banerjee, K.; Datta, D. *New J. Chem.* **2007**, *31*, 832. (c) Batsanov, S. S. *J. Mol. Struct.* **2011**, *990*, 63.

(26) Kwart, H. *Acc. Chem. Res.* **1982**, *15*, 401.

(27) (a) See, for example, the following: Thewalt, U.; Woehrl, T. *J. Organomet. Chem.* **1994**, *464*, C17. (b) Chen, J.; Kai, Y.; Kasai, N.; Yasuda, H.; Yamamoto, H.; Nakamura, A. *J. Organomet. Chem.* **1991**, *407*, 191.

(28) Kubas, G. J. *Metal Dihydrogen and  $\sigma$ -Bond Complexes*; Kluwer Academic: New York, 2001; Chapter 9.